Mohamed Khider University of Biskra
Faculty of exact sciences and natural and life sciences
Material sciences department

MASTER MEMORY

Material sciences
Physics
Energy physics and renewable energies

Réf. : Entrez la référence du document

Presented by:
HERIBI OUISSAL LATRA
On : 20/06/2023

Effect of PH precursor on properties of TiO_2 thin films deposited by ultrasonic spray process and their photocatalytic applications

---

Jury:

Mrs. Marmi Saida	MCA	University of Biskra	President
Mr. Attaf Abdallah	Pr	University of Biskra	Supervisor
Mrs. Saidi Hanane	Pr	University of Biskra	Examiner

Academic Year: 2022/2023

بِسم الله الرحمن الرَّحيم

﴿ يَرْفَعِ اللَّهُ الَّذِينَ ءَامَنُواْ مِنكُمْ

وَ الَّذِينَ أُوتُواْ الْعِلْمَ دَرَجَٰتٍ ﴾

صدق الله العظيم

إهداء

{ و آخِرَ دَعْوَاهُم أَنِ الْحَمْدُ لِلهِ رِبِّ الْعَالَمِينَ }

وَتَدعو أنْ لا يكون طريقك وَعِرًا؛ لتَّنجو، فيكون وَعِرًا، وتَنجو !لتَعلمْ أَنَّ النَّجاةَ مِن الله، لا مِنْ الطَّريق

لم تكن رحلتي قصيرة ، و لم يكن حلمي قريبا ، و لا طريقي كان محفوفا بالتسهيلات ، و لكن عظُم المراد فهانت الطريق ، و كان الوصول على قدر المشقة و الصبر مهيبا و عظيما .

أهدي فرحتي التي انتظرتها طويلا و ثمرة جهدي

إلى رفيق دربي و من علمني أن الدنيا كفاح، أعظم رجل في الكون أبي الغالي

صالح

إلى مأمني و أماني، صديقتي و نور دربي أمي الغالية

نور الهدى

إلى مؤنساتي الغاليات ، زهرات حياتي، اخواتي

رملة ، ياسمين ، نسرين

إلى سندي في الخطوة الأولى و الأخيرة، بهجة قلبي **خالاتي و اخوالي**

من كان أخا حنون لي و قوتي في ضعفي، **عمي الغالي**

إلى فقيدتنا هذا العام، طيبة القلب و جميلة الروح زوجة خالي الغالية **عائشة** رحمة الله عليها

Acknowledgment

In the first place, I offer special thanks and appreciation to my supervisor in this work, my honorable professor Attaf Abdallah, a professor at the University of Biskra, for his tremendous efforts that he made with me to make this dissertation a success. and for his moral support and encouragement throughout the completion of this work, for his confidence in me, and for the opportunities he has given me to do an excellent master dissertation work, thank you very much.

I sincerely thank Mrs. Marmi Saida, a teacher at the University of Biskra who did me the honor of chairing the jury.

My most laudatory thanks to Mrs. Saidi Hanane, professor at the University of Biskra, who kindly accepted to be part of the jury and to examine my work.

Special thanks to the Ph.D student Okba Ben khetta, who was a support and companion on the journey of this work.

I am grateful and so thankful to Dr. Boubeche Rahma and all the members of Songshan lake materials laboratory, at University Innovation Park, Dongguan, Guangdong, China, for all the characterizations measurement of our samples in this study.

I genuinely appreciate the moral support from all of my professors during my 5 years of study, especially Dr. Ouhabab Noureddine, and Dr. Abdeslam Nora Amele, for all their moral and motivating encouragement, thank you so much.

I also want to thank our team in thin films laboratory: Djehiche.N, Douba.O and all.

Contents

Figure list :

Table list :

General introduction

Thin films of transparent conductive oxides (TCOs) have been the focus of several studies due to their attractive optical and electrical features. The most attractive TCOs are ZnO, SnO_2, In_2O_3, and TiO_2, this last has been widely investigated for its promised characteristics, given that it has versatile qualities including a high refractive index, a wide band gap (3.2 eV), high physical and chemical stability, and a non-toxic nature. TiO_2 thin films are used in a variety of fields, including photo-detectors, gas sensors, electronics, waste water treatment, and photocatalysis. [1,2]

The objective of this master dissertation is to elaborate thin films of TiO_2 using the ultrasonic spray pyrolysis technique.

In this work, we will study the effect of Potential hydrogen PH precursor on the properties of titanium dioxide TiO_2 thin films and their photocatalytic application. For this, we made a serie of samples deposited on the glass substrates, and to improve the crystallinity of our samples, we will anneal it at 600°C.

This work is divided into four chapters:

- In the first chapter, we will present a bibliographic study about transparent conductive oxides. We then give an overview of the general properties of titanium dioxide (structural, optical, and electrical) and some applications of this oxide, and at the end, we will discuss an overview of thin films.

- In the second chapter, we will describe some different deposition processes, that can be used to obtain thin films, we will also present the methods of structural, morphological, and optical characterizations in this work.

- The third chapter is devoted to the discussion and interpretation the results of structural, and morphological characterizations of the elaborate thin films obtained.

- The fourth chapter contains a discussion of the optical characterizations of our thin films and the results of the photocatalytic application.

At the end of this work, we have a general conclusion and perspectives.

Chapter 1 :

Overview of Titanium dioxide (TiO_2) and thin films

In this chapter, we present a bibliographic study about transparent conductive oxides TCOs, followed by an overview of titanium dioxide TiO_2 and certain properties and applications of this oxide, and at the end we will discuss an overview of thin films.

I.1. Transparent Conductive Oxides (TCOs)

The term "transparent conductive oxides" (TCOs) refers to a class of materials that exhibit both transparency and conductivity. The transparent characteristic of TCOs is attributed to their high optical transmission in the visible spectrum, which necessitates an energy gap of more than 3.3 eV. According to the conducting characteristics, TCOs exhibit strong electrical conductivity in the region of 1 to 10^4 S cm^{-1}. [3]

Solar cells, heat mirrors, smart windows, touch screens, and gas sensors are just a few of the many uses for transparent conductive oxides (TCOs), also known as transparent electrodes for flat panel displays, liquid crystal displays (LCD), and organic light emitting displays (OLED). [4]

I.1.1. Criteria of choice

The criteria for choosing a TCO depend on various material-related factors, such as the toxicity of the material, thermal and chemical stability, and production costs. The most attractive TCOs are CuO, ZnO, SnO_2, In_2O3 and **TiO_2**, this last has been widely investigated for its promised characteristics. [5,6].

In this study, our choice is **Titanium dioxide TiO_2.**

I.2.Titanium dioxide

Titanium dioxide TiO_2 is one of the most interested materials, especially in the applied side by researchers, because of its distinctive properties, its scientific and technological importance, and its ability to form in many forms under different chemical conditions. [7,8]

I.2.1. Choice of Titanium dioxide

Titanium dioxide is a very important semiconductor, when its composition is stoichiometric, TiO_2 behaves like an insulator, while a few defects are enough to make it an n-type semiconductor (oxygen vacancy, interstitial titanium atoms), it's a chemically stable, non-toxic, non-volatile material, non-flammable and biocompatible, It presents for the visible light spectrum a very high diffusion coefficient without absorption zone due to its particularly high refractive index and its insensitivity to visible light. The properties of TiO_2 depend on several parameters, namely the nature of the phase, crystallinity, and chemical composition. [9]

I.2.2. Properties of Titanium dioxide

I.2.2.1. Structural properties

Under different conditions of pressure and temperature, TiO_2 has several allotropic phases, it is known that it has three main polymorph phases: **anatase**, **rutile**, and **brookite**, which are obtained when samples are prepared at relatively low pressures [7], which is what interests us in our study.

- **Brookite phase:**

The unit cell of brookite has an orthorhombic crystalline structure. The parameters of the lattices are a = 0.9182 nm, b=0.5456 nm, and c = 0.5143 nm. The space group Pbca describes the symmetry of the atom distribution in a unit cell. A deformed octahedron with a titanium atom located close to the center and oxygen atoms in the vertices can be used to represent the local atom distribution of the structure as depicted in figure I.1. As a bulk material the brookite phase is the rarest and hardest to synthesize in a laboratory setting of all the natural TiO_2 polymorphs. [10,11]

The following figure shows the brookite phase structure:

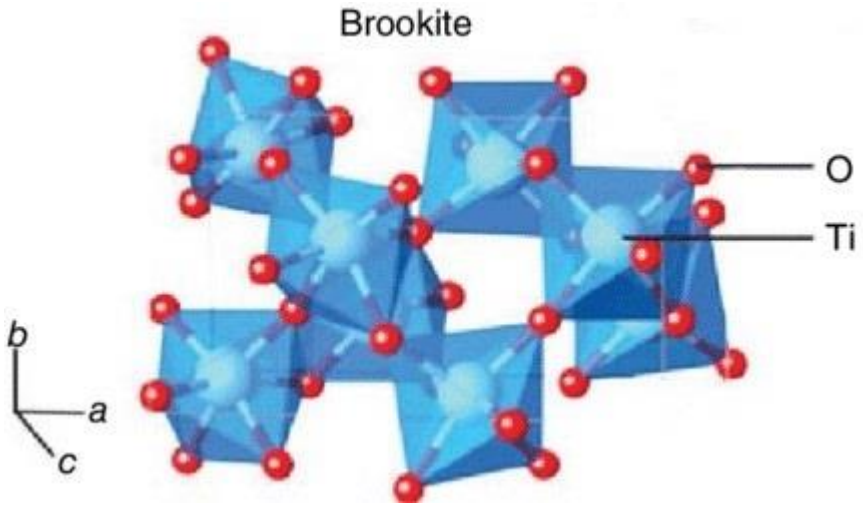

Figure I. 1 Brookite phase structure of TiO_2 [12]

Rutile phase:

The crystal structure of rutile is characterized by tetragonal symmetry and belongs to space group $P4_2$=mnm. The lattice constants are a = 0.4594 nm and c = 0.2958 nm. As a bulk material the preferred growth direction of the crystals is (110) surface. For optical uses rutile is desirable. [11,13]

And figure I.2 shows the Rutile phase structure:

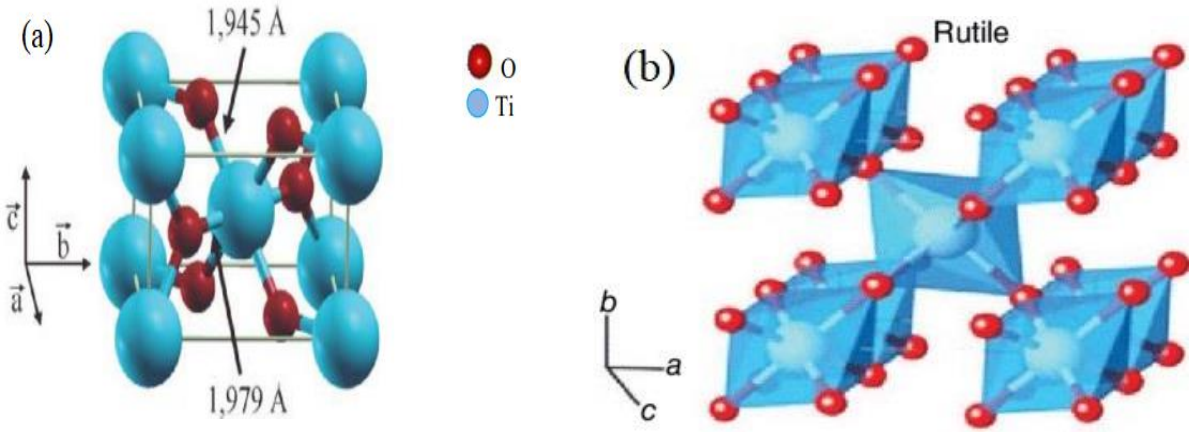

Figure I. 2 (a) bonds of rutile structure, (b) rutile phase structure [12]

- **Anatase phase :**

Anatase is a form of natural titanium oxide. The unit cell of anatase is also of tetragonal symmetry with the parameters a=b= 0.37710 nm and c=0.9430 nm, it belongs to space group $I4_1/amd$.[13]

And figure I.3 shows the Anatase phase structure:

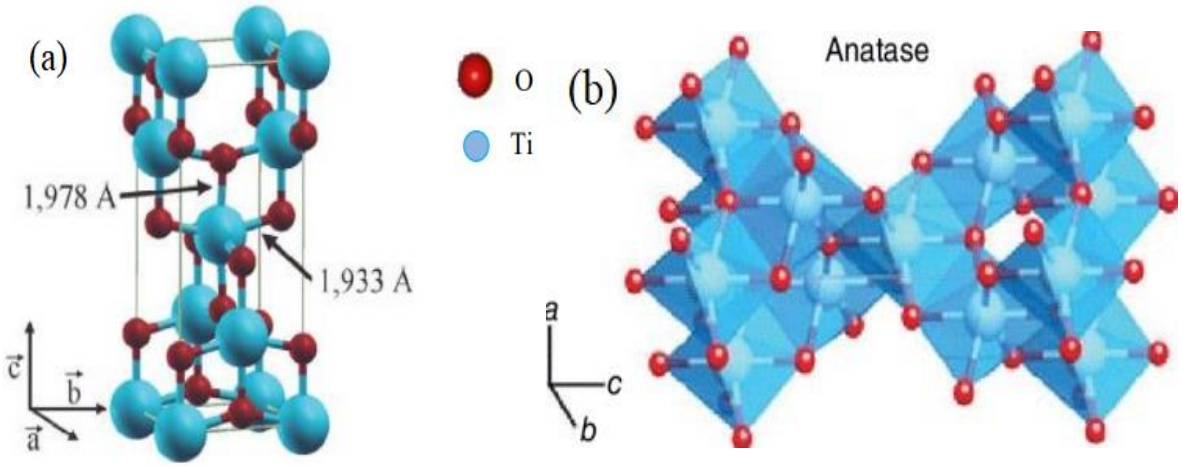

Figure I. 3 (a) bonds of anatase structure, (b) anatase phase structure [12]

The corresponding table summarizes the structural properties of the three phases:

Table I. 1 The structural properties of the three phases [14]

Properties	Brookite	Rutile	Anatase
Crystalline structure	Orthorhombic	Tetragonal	Tetragonal
Number of TiO_2 molecule per cell	8	4	2
Cell parameters (Å)	a = 9.184 b = 5.447 c = 5.145	a =b= 4.594 c = 2.958	a = b=3.785 c = 9.514
Density ($g.cm^{-3}$)	4.12	4.24	3.89
Space group	Pbca	$P4_2/mnm$	$I4_1/amd$

- **Transition from one phase to another:**

The transformation temperatures change according to the nature of the titanium oxide. In the bulk state, anatase irreversibly transforms into rutile at a temperature of about 820°C. On the other hand, the transformation temperature varies in thin films, because it depends on the method of composition used and even on the conditions of the experiment and the products. Can be introduced that, at a temperature above 625 ° C, the anatase and brookite completely convert to rutile, knowing that brookite converts to rutile faster than anatase, the transformation temperature can also be adjusted by adding impurities to TiO_2. For example, the anatase phase completely disappears at temperatures around 530 °C, 680 °C, and 830 °C for powder samples containing vanadium, molybdenum, and tungsten, respectively. [7]

The following figure I.4 shows the reaction boundaries of phase transitions:

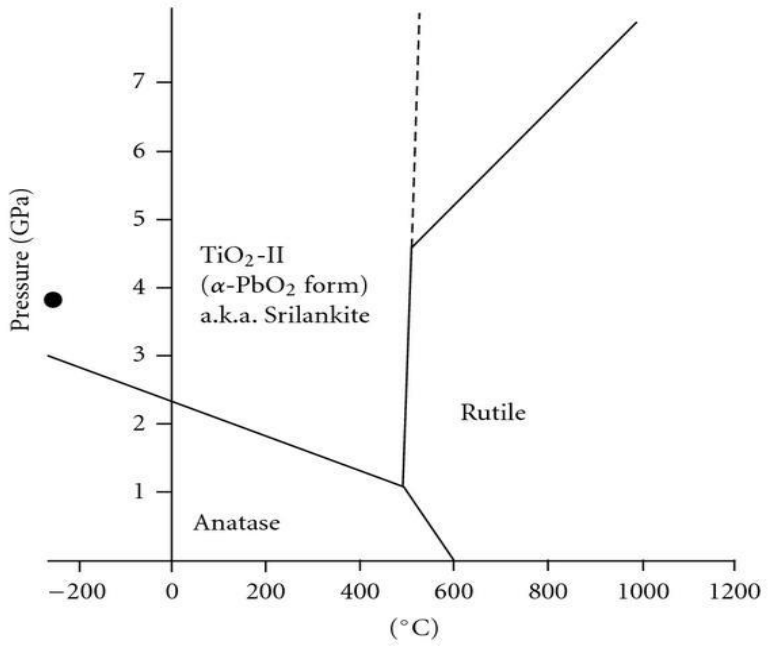

Figure I. 4 Reaction boundaries of phase transitions of TiO_2 [15]

I.2.2.2. Optical properties

TiO_2 presents for the UV-Visible spectrum a high transmission coefficient in the visible range as shown in figure I.5:

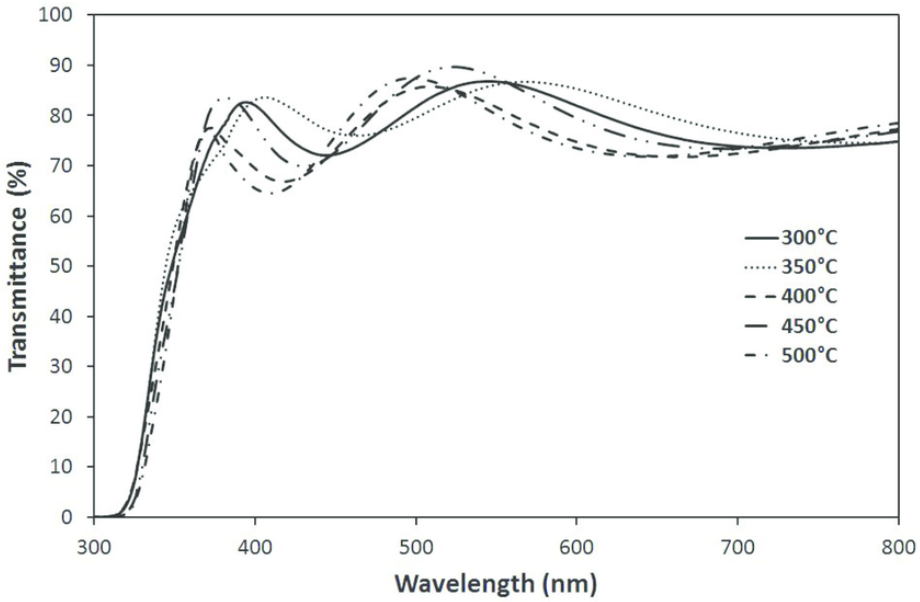

Figure I. 5 Effect of annealing on transmittance of TiO_2 [16]

And the following table presents a comparison of the optical properties of TiO_2 phases:

Table I. 2 Comparison of the optical properties of TiO_2 powder for each phase [14]

Properties	Brookite	Rutile	Anatase
Gap energy	3.14	3.03	3.20
Refractive index	2.55	2.70	2.57

I.2.2.3. Electronic properties

TiO_2 is an N-type semiconductor, figure I.6 shows that the BV (valence band) is mainly dominated by the 2p orbital of the O atom. The 3d orbital of the titanium atom is at the bottom of the BC (conduction band). This presence of oxygen in the BV justifies the fact that TiO_2 is an N-type semiconductor because for each oxygen missing in the structure, there are 2 free electrons compensated by the Ti^{3+} centers.

For the anatase phase, the forbidden band is 3.2 eV, which means that the TiO_2 anatase absorbs photons with a wavelength less than or equal to 380 nm. TiO_2 anatase, therefore, absorbs in the UV range of the solar spectrum, which corresponds to less than 6% of solar energy. [17]

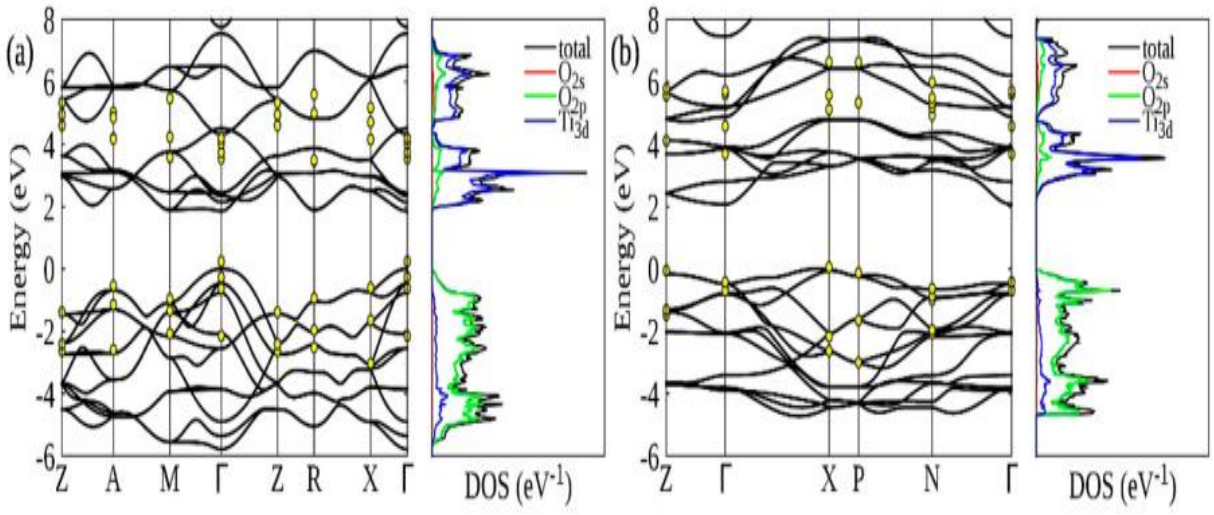

Figure I. 6 Band structure and the corresponding DOS of (a) rutile, (b) anatase [18]

I.2.2.4. Photocatalytic properties

The photocatalytic properties of TiO_2 result from the creation of photogenerated charge carriers (hole and electrons), which happens when ultraviolet (UV) light corresponding to the band gap (hν≥ 3.20 eV at λ ≤ 380 nm) is absorbed, which excites an electron from the ground state of the valence band to the conduction band (e^-_{CB}), and creating a hole (h^+_{VB}) in the valence band, figure I.7 is a schematic representation of this process. The electron and the hole participate in redox reactions with substances that are adsorbed on the TiO_2 surface, including water, or oxygen. resulting in the creation of the superoxide radical anion (O_2^-•) and the hydroxyl radical (OH•) (Equation (2) and Equation (4), respectively). The valence band hole (h^+) is highly oxidizing while the conduction band electron (e^-) is highly reducing. Equation (6) explains how O_2^-• combines with H^+ to create the hydroperoxyl radical (OOH•), and equation (8) explains how it may also react with itself to create H_2O_2. Equations (3), (5), and (7) show that the radicals generated by photocatalysis are strong oxidants that may effectively oxidize organic molecules, resulting in the mineralization of mineral salts, CO_2, and H_2O. [19-21]

Below is a list of the photocatalysis reactions for TiO_2 from (1) to (8) [20]:

$$TiO_2 + h\nu \longrightarrow e^-_{CB} + h^+_{VB} \quad \text{(I.1)}$$

$$HO^- + h^+_{VB} \longrightarrow HO^\bullet \quad \text{(I.2)}$$

$$H_2O + h^+_{VB} \longrightarrow HO^\bullet + H^+ \quad \text{(I.3)}$$

$$O_2 + e^-_{CB} \longrightarrow O_2^{\bullet -} \quad \text{(I.4)}$$

$$O_2^{\bullet -} + pollutant \longrightarrow H_2O + CO_2 \quad \text{(I.5)}$$

$$O_2^{\bullet -} + H^+ \longrightarrow OOH^\bullet \quad \text{(I.6)}$$

$$OOH^\bullet + pollutant \longrightarrow H_2O + CO_2 \quad \text{(I.7)}$$

$$OOH^\bullet + OOH^\bullet \longrightarrow H_2O_2 + O_2 \quad \text{(I.8)}$$

The following figure explain the principal of photocatalytic process in a TiO_2 thin films:

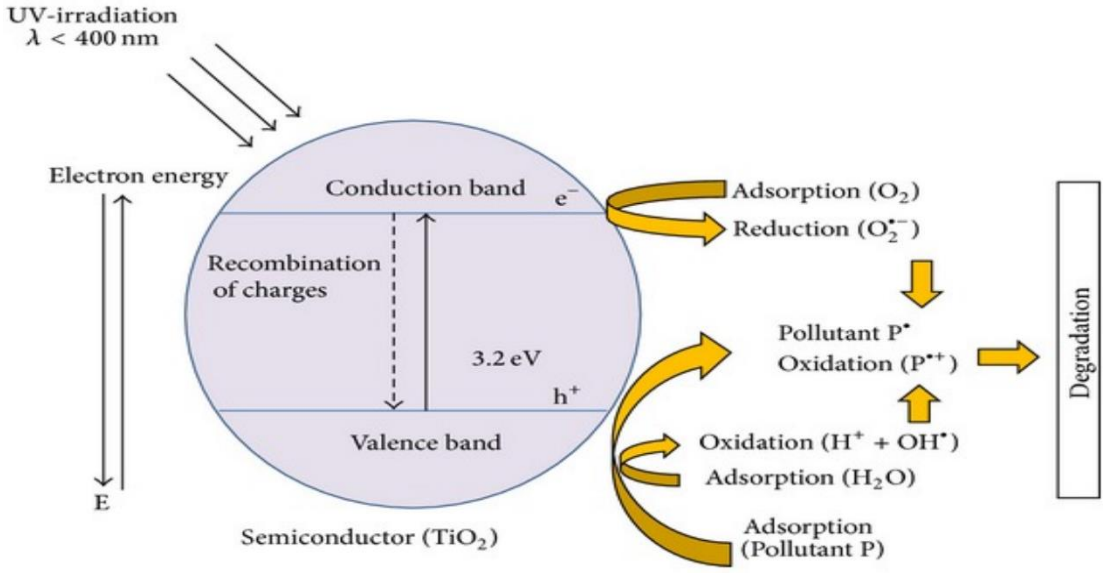

Figure I. 7 Diagram of the photocatalytic process in a anatase TiO_2 thin films [22]

- **Phenomenon of super-hydrophilicity**:

There is a phenomenon called "super-hydrophilicity" which has been demonstrated on TiO_2. When the contact angle of TiO_2 with water becomes close to zero, the surface of the material no longer retains water and we speak of "super-hydrophilicity". When the TiO_2 surface is exposed to UV radiation, the contact angle with water gradually decreases. After a sufficiently long exposure to light, the surface becomes "super-hydrophilic". This particular character can be obtained for one or two days. This type of photocatalyst is the only one known with a semi-permanent super hydrophilic property. This property led to the development of technologies for self-cleaning and anti-fog materials. [23,24]

Titanium dioxide TiO_2 is elaborated in several forms among them: powders [25,26], nanotubes [27,28], nanoparticules [29], and **thin films** [10,30,31] which is the type chosen for TiO_2 formation in this study.

I.3. Thin films

I.3.1. Definition of thin film

A thin film is a thin layer of a substance deposited on a "substrate," a substance whose thickness has been significantly reduced and can vary between a few "nm" to a few "µm", the majority of the physical properties are disturbed as a result of the limited distance between the two boundary surfaces.

The fundamental difference between a material in its bulk state and one in thin films is related to the fact that in the massive state, limits are typically ignored for good reasons, whereas in a thin film, effects related to limiting surfaces which are dominating. [32,33]

I.3.2. Thin films growth mechanisms and modes

I.3.2.1. Thin films growth mechanisms

The following are the essential steps in every thin film deposition procedure: [34]

- The arrival or adsorption of atoms (or molecules) on the surface of the substrate.
- Surface diffusion of atoms.
- The interaction between the deposited atoms and/or those of the substrate for the formation of stable bonds.
- Nucleation.
- coalescence.
- Volume growth.

The process of thin films formation can be described as a statistical progression of nucleation, followed by growth through surface diffusion and the creation of small islands. These islands then grow in size until they form larger islands, which ultimately fuse together to form a continuous layer by filling the gaps between them.

I.3.2.2. Growth modes

Depending on the thermodynamic parameters of the deposition and the substrate surface, the steps of nucleation and islands growth can be described as three modes: [19]

- Islands mode (3D or multi-layered) called Volmer-Weber (VW).
- Layer-by-layer (2D) mode called Frank-van der Merwe (FvdM).
- Mixed mode called Stranski-Krastanov (SK).

Three modes of growth are schematically illustrated in the figure:

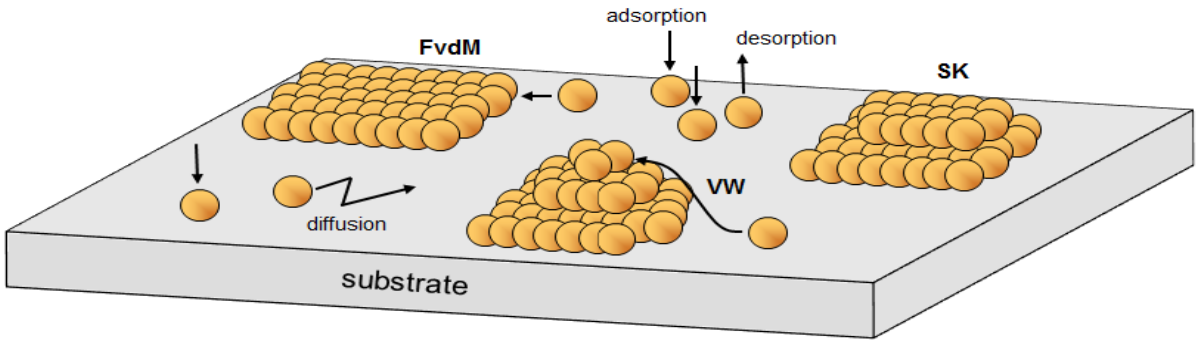

Figure I. 8 Different thin films growth mechanisms [35]

The scientific, industrial and high-tech applications of titanium dioxide are numerous, thus **TiO_2 thin films** are widely used in various applications.

I.3.3. Applications of TiO_2

I.3.3.1. Application in optics

Titanium dioxide coatings are ideal for optical guidance because they can for example, increase signals in films doped with rare earth ions or change the surface refractive index of glasses. [17]

I.3.3.2. Application in solar cells (Dye Sensitized Solar Cell)

Michael Gratzel made a significant discovery relating to the usage of TiO_2 in photovoltaics. Only the monolayer of dye molecules in contact with TiO_2 is capable of absorbing light. Barely 1% of the incident light is absorbed on a flat surface. Use a TiO_2 coating comprised of TiO_2 nanoparticles to improve absorption. The roughness of the surface is substantially higher. Thus, when in contact with the electrolyte, more molecules can be adsorbed on the TiO_2 surface. [18]

I.3.3.4. Photocatalytic application

Using photocatalysis to degrade or decompose pollutants in the air and on water is a novel method. Highly active photocatalytic TiO_2 thin films are desired in a variety of applications, particularly in pollution reduction and self-cleaning technologies because of their capacity to break down organic molecules, which makes them useful for water, air, and surface cleaning as well as the purification of pollutants. The photocatalytic inactivation of bacteria has also been investigated, because it can eliminate a variety of microorganisms, including bacteria and viruses, or for the conversion of CO_2. [17,18,36]

In order to reduce the spread of airborne toxins and allergens, such as COVID-19 viruses [37], photocatalytic coatings on high-touch surfaces will be applied in public places, including hospitals, public transportations, athletic centers, schools, acute care facilities, airports, arenas, and other locations. [38]

I.3.3.5. Photocatalytic hydrogen production

The photocatalytic production of hydrogen presents certain difficulties related to the use of visible light, the limited quantum efficiency, and the photodegradation problems of the catalyst. Although TiO_2 is one of the most used for this application due to its appropriate conduction band value, much remains to be done to develop new photocatalytic nanomaterials that are truly effective for the production of hydrogen. Various photocatalysts have been considered to perform the decomposition of water to produce hydrogen. However, their efficiency is still too low. The combination of TiO_2 and carbon nanomaterials could help improve this efficiency. [18]

We can produce TiO_2 thin films with a variety of **deposition methods**, due to its wide and different applications, which we will see it in chapter 2.

Chapter 2 :

Deposition techniques and characterization methods for thin films

This chapter contains the deposition techniques of thin films, whether physical or chemical types, followed by the characterization methods.

II.1. Deposition techniques of thin films

Deposition techniques are generally classified into two main families: chemical and physical techniques as shown in figure II.1:

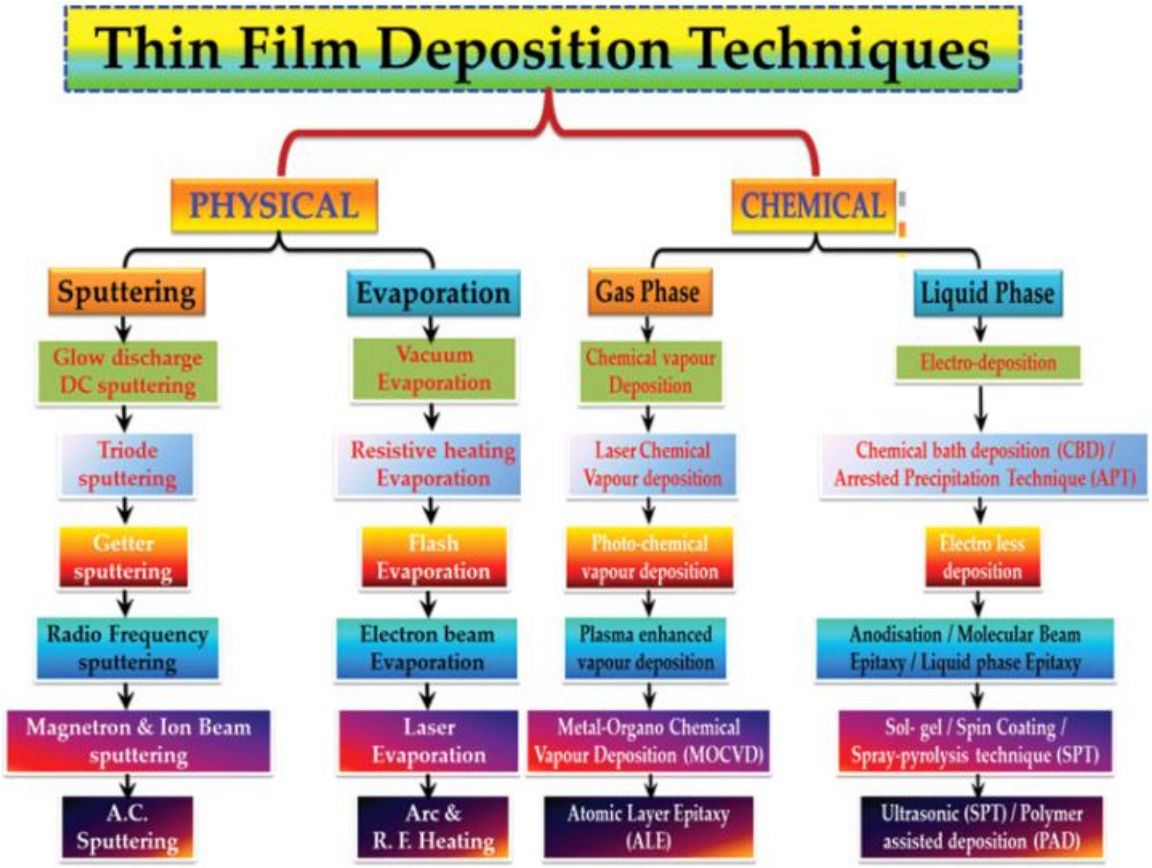

Figure II. 1 Flowchart of the Thin Films Deposition Techniques [39]

TiO_2 thin films have been deposited using a variety of techniques, Among the chemical techniques: the sol-gel process [10], and the atomization technique known as spray pyrolysis technique [40,41]. Pulsed laser ablation (PLD) [42] and sputtering [43] are the two most used physical techniques for the deposition of TiO_2 thin films. [13]

II.1.1. Choice of a deposition technique

The choice of the deposition technique is predominantly determined by the intended quality and the application of the produced thin films. Initially it is first important to determine the technique that will be used to produce the substance that will be deposited. The factors that condition the choice of technique are [44]:

- The nature of the material to be deposited.
- The desired deposition rate and layer thickness.
- Constraints imposed by the substrate.
- The desired stoichiometry.
- The adhesion of the deposit to the substrate.
- The reproducibility and the cost of realization.

The **ultrasonic spray pyrolysis technique** which was used in this dissertation will present in some detail.

II.1.2. Physical deposition techniques

II.1.2.1. Pulsed laser ablation technique

As shown in the figure below, a lens outside the vacuum chamber focuses the pulsed laser beam onto the target. When the laser fluence rises beyond a threshold value (the Buence is the laser pulse energy per unit area at the target), a bright plume of material is generally discharged to the target surface and collected on an appropriately placed and heated substrate. Provision is made to rotate the target, change the distance between the target and its substrate, and change the distance between the target and its lens. [45]

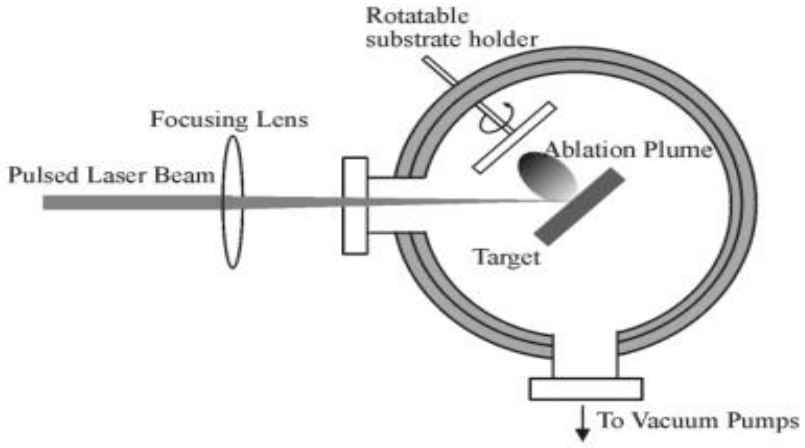

Figure II. 2 Schematic diagram of an apparatus for PLA of a solid target with deposition on an on-axis mounted substrate [46]

II.1.2.2. Sputtering technique

The working principle of the PVD-sputtering process is that a substrate is made as anode and the deposition or target material is made as cathodes, which are separated by a distance in the range of 5–10 cm in a chamber having a vacuum in the range of 10^{-6} to 10^{-10} torr. The flow of an inert gas such as argon (Ar) is continuously provided to the vacuum chamber in which its molecules become positively charged ions ejecting electrons under applied high pressure and voltage. The ejected electrons may further ionize other gas atoms to sustain the glow discharge and create a cascading process until all the gas molecules ionize. These ions strike the cathodic deposition material-ejecting molecules from its surface by transfer of their momentum. This phenomenon is known as sputtering. [47]

Following figure shows working principle of PVD sputtering process:

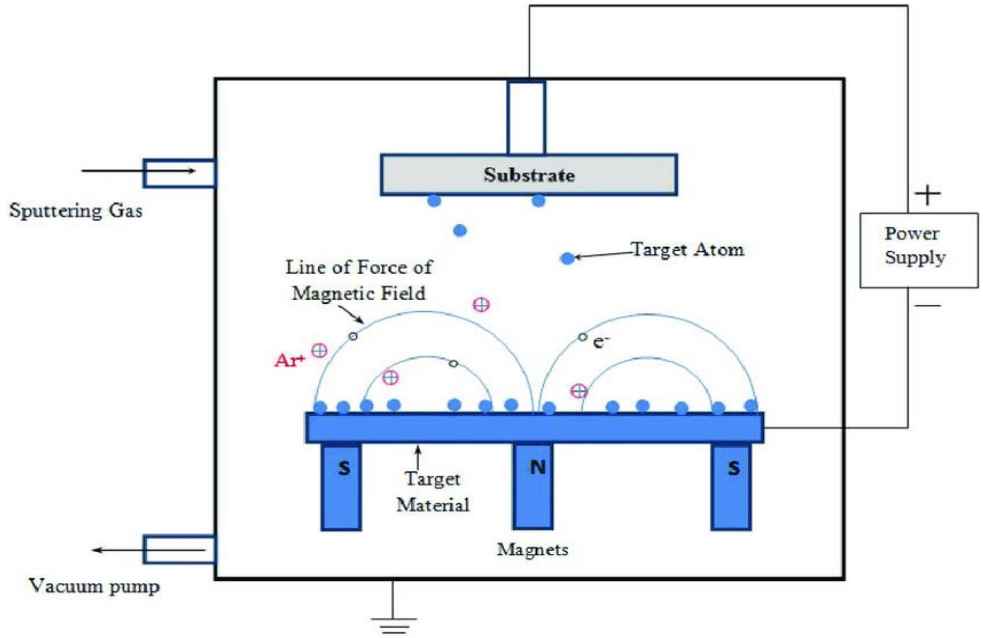

Figure II. 3 Working principle of PVD sputtering process

II.1.3. Chemical techniques

II.1.3.1. Sol-gel technique

The sol–gel process is a chemical synthesis technique based on the conversion of a liquid into a solid phase by a series of chemical reactions of the hydrolysis and condensation type of the molecular solution of extreme purity at much lower temperatures than is possible by traditional methods of preparation. In this method, the molecular precursor (usually metal alkoxide) is dissolved in water or alcohol and converted to gel by heating and stirring by hydrolysis/alcoholysis. Since the gel obtained from the hydrolysis/alcoholysis process is wet or damp, it should be dried using appropriate methods depending on the desired properties and applications of the gel. [30,48,49]

Figure II.4 shows sol-gel process:

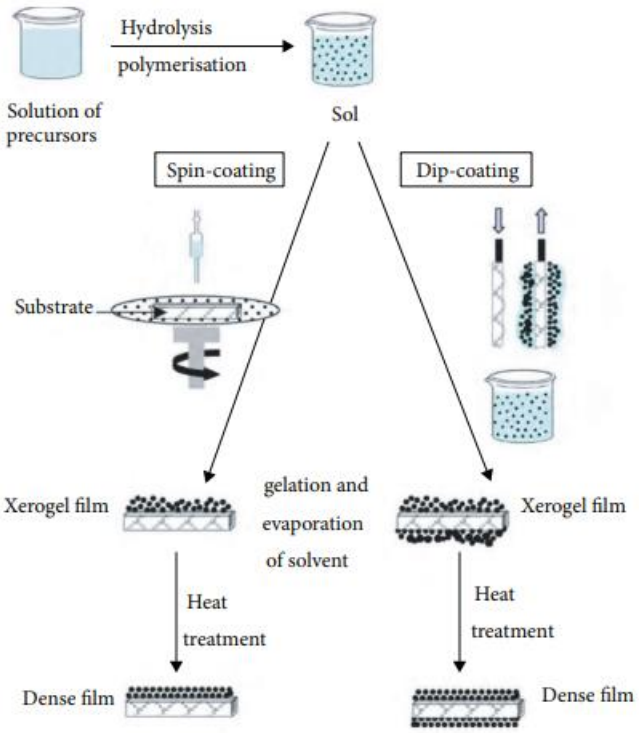

Figure II. 4 Schematic of sol-gel process [49]

II.1.3.2. Spray pyrolysis technique

II.1.3.2.1. Definition

Spray pyrolysis is a word consists of: spray and pyrolysis.

- Spray: is an English word that indicates jet of a liquid in fine droplets, launched by a sprayer.
- Pyrolysis: is a process by which a solid (or a liquid) undergoes, under the effect of heat and without interaction with oxygen or any other oxidants, a degradation of chemical products to smaller volatile molecules. [19]

The technique of spray pyrolysis is an adaptable processing method for the preparation of single layer and multi-layer films in the form of dense or porous layers, ceramic coatings and powders of various materials. [34]

It has many advantages among them [50,51]:

- Possibility of depositing a wide choice of materials.
- A wide choice of precursors is possible, the compound must be soluble in a solvent, so the solution can be atomized.
- Simple method of adding the precursor by means of a spray.

- High growth rate because the mass transport of the precursor can be very high.
- Simply controllable reaction environment, under neutral gas or under air at atmospheric pressure.
- Ease of construction of reactors of this type.
- Open-atmosphere process.
- Open-reaction chamber.
- Adjustability during the deposition.
- Accessibility for observing the deposition procedure.
- The capability of the multi-layer preparation that is very appealing for fabricating functionally graded layers.

Typical spray pyrolysis equipment consists of [34]:

- An atomizer.
- Precursor solution.
- Substrate heater.
- Temperature controller.

II.1.3.2.2. Principle of the Pyrolysis spray process

Its general principle is based on the spraying of a mist of a solution containing all the reagents capable of combining to give the desired compound, using an atomizer, on a heated substrate. The small droplets of the sprayed solution are generated by an aerosol generator (atomizer) under the pressure of a gas. The temperature of the substrate allows the activation of the chemical reaction between the compounds and thus ensures complete evaporation solvents at the substrate level during the formation of the layer of the desired compound. [4]

II.1.3.2.3. Deposition process

These processes are based on the spraying of the starting solution, the transport and the evaporation of the solvents, the diffusion and the decomposition of the precursors on the substrate. Then thin films deposition can be summarized as follows: aerosol generation, aerosol transport and precursor decomposition.

1. Generation of the aerosol:

Two methods are generally used to spray the solution containing the source material [44]:

- **Pneumatic spray**: the production of the mist is carried out by a compressed gas which causes the liquid to burst.

- **Ultrasonic spray**: the aerosol is generated from the high frequency vibrations produced within the solution, and localized towards the free surface of the liquid.

When an ultrasound beam is directed towards a gas-liquid interface, a geyser is formed whose height is a function of sound intensity. This geyser is accompanied by the production of an aerosol, resulting from the vibrations generated at the surface of the liquid and from the cavitation at the gas-liquid interface. This is the pyrosol process.

Figure II.5 shows the schematic of ultrasonic spray procedure:

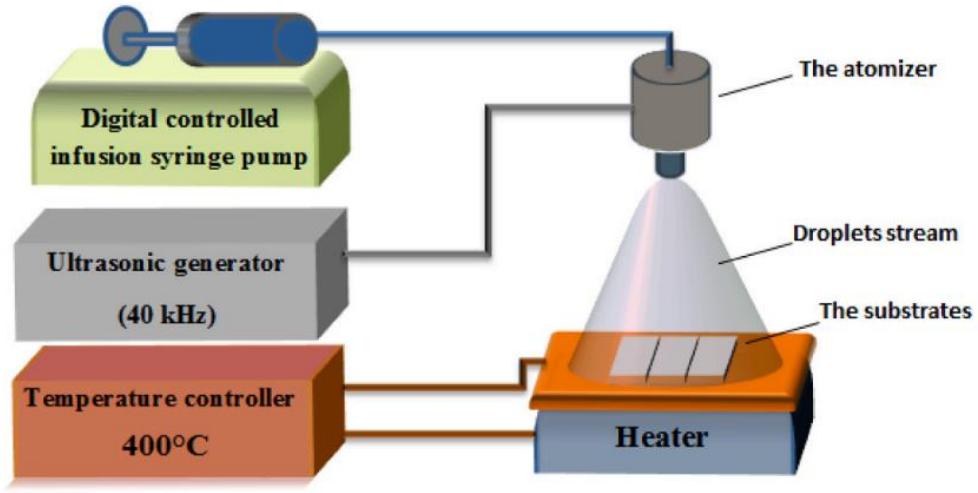

Figure II. 5 Schematic of ultrasonic spray procedure [52]

2. Transport of the aerosol:

After the droplet leaves the atomizer, it travels through room temperature with an initial velocity determined by the atomizing nozzle. In the form of an aerosol, the droplets are transported with the aim of allowing as many droplets to reach the surface. When the droplet passes through the surrounding air, four forces acting simultaneously on it describe its path. These forces are gravitational, electric, thermophoretic and the Stokes force. [19]

3. Decomposition of the precursor:

Several processes occur when a droplet hits the surface of the substrate. the following processes that occur with increasing substrate temperature. When the substrate temperature is low (process A), the droplets splash against the surface and decomposes (figure II.6). Higher temperatures (process B) cause the solvent to entirely evaporate during the droplet's flight before the dry precipitate contacts the substrate and begins to decompose. At even greater temperatures (higher than in the later situation) the solvent also evaporates before the droplet touches the substrate, the solid precipitate then melts and vaporizes without breaking down, and the vapor diffuses to the substrate to go through a CVD process (process C). The precursor vaporizes at the highest temperatures (process D) before it reaches the substrate, and as a result, the solid particles are created after the chemical reaction in the vapor phase. [34]

Figure below shows the decomposition processes of spray pyrolysis:

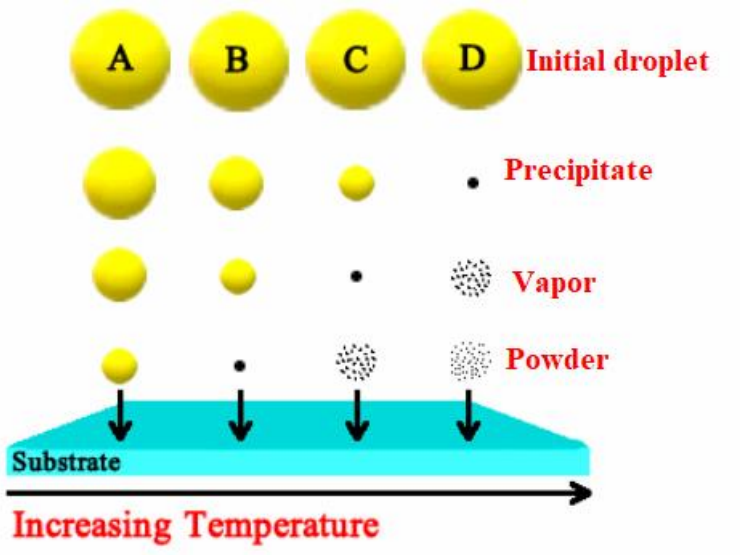

Figure II. 6 Different decomposition processes of spray pyrolysis [53]

II.2. Thin films characterization methods

The analysis methods used in the study, which we will discuss bellow, are: X-ray diffractometer (XRD), UV-visible spectrophotometer, Scanning Electron Microscopy (SEM), Raman, Attenuated Total Reflectance Fourier Transform Infrared spectroscopy (ATR-FTIR), Photoluminescence (PL). All the characterization equipment used in this study was in **China**.

II.2.1. structural properties

II.2.1.1.X-ray diffractometer (XRD) method

X-ray diffraction (XRD) is A potent nondestructive method for characterizing crystalline materials. It offers details on crystal textures, optimum orientations for crystals, and other structural factors like average grain size, crystallinity, strain, and crystal defects. It also offers details on structures and phases. X-ray diffraction peaks are produced by constructive interference of a monochromatic beam of X-rays scattered at specific angles from each set of lattice planes in a sample (Figure II.7). The distribution of atoms within the lattice controls the peak intensities. As a result, the X-ray diffraction pattern represents a signature of periodic atomic arrangements in a given material. [54]

The interaction of the incident rays with the sample results in constructive interference when the conditions comply with Bragg's law [32]:

$$n\lambda = 2d_{hkl}sin\theta \qquad \text{(II.1)}$$

Where: n is the order of diffraction.

λ is the wavelength of the X-rays.

d_{hkl} is the interplanar spacing generating the diffraction.

θ is the diffraction angle (Bragg angle).

This law relates the lattice spacing and diffraction angle of a crystalline sample to the wavelength of electromagnetic radiation, and this is what the following picture shows:

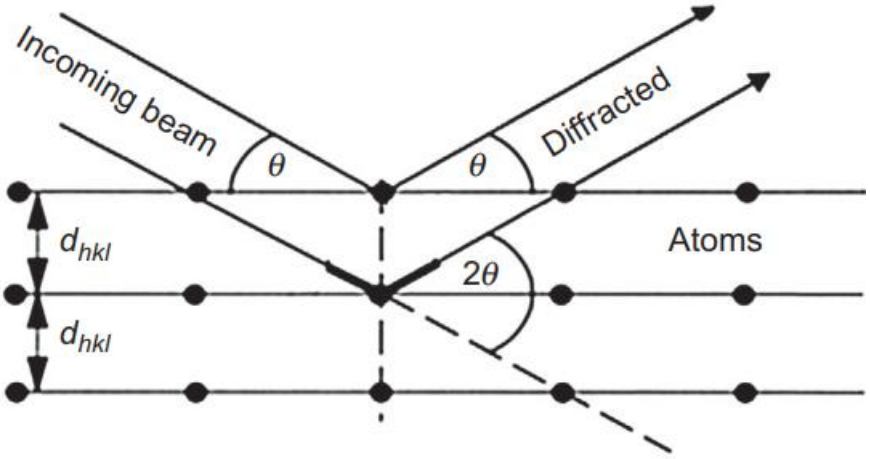

Figure II. 7 Reflection of X-rays from two planes of atoms in a solid [55]

II.2.1.1.1. Crystallite size and dislocation density

Using the XRD spectra, we can use the Debye-Scherrer formula to determine the crystallite size [52]:

$$D = \frac{0.94\lambda}{\beta cos\theta} \qquad \text{(II.2)}$$

Where: λ is the x-ray wavelength (Cu Kα, λ = 1.540593 Å).

β is the full width at half-maximum intensity (FWHM) of the peak.

θ is the Bragg angle.

The FWHM shown in figure bellow:

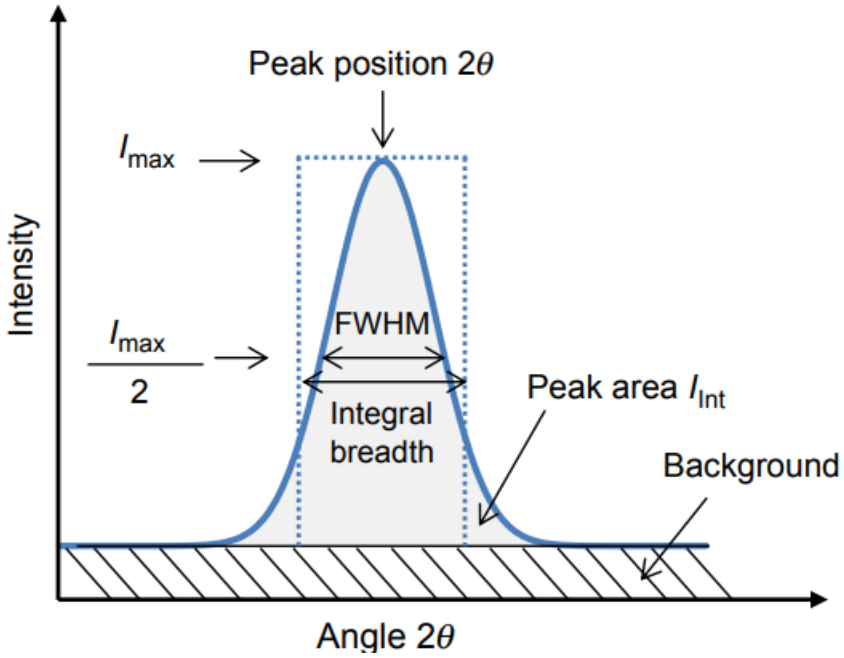

Figure II. 8 The width at half height of the peak (FWHM) [55]

The dislocation density (δ) given in equation II.3 is defined as the length of dislocation lines per unit area in the film, and can be calculated using the crystallite size (D): [56]

$$\delta = \frac{1}{D^2} \qquad \text{(II.3)}$$

II.2.1.1.2 Micro-Strain

We calculate strain from the following equation [57]:

$$\varepsilon = \frac{\beta}{4\tan(\theta)} \qquad \text{(II.4)}$$

structural characterization of the samples was determined by Rigaku SmartLab Diffractometer **{China}**:

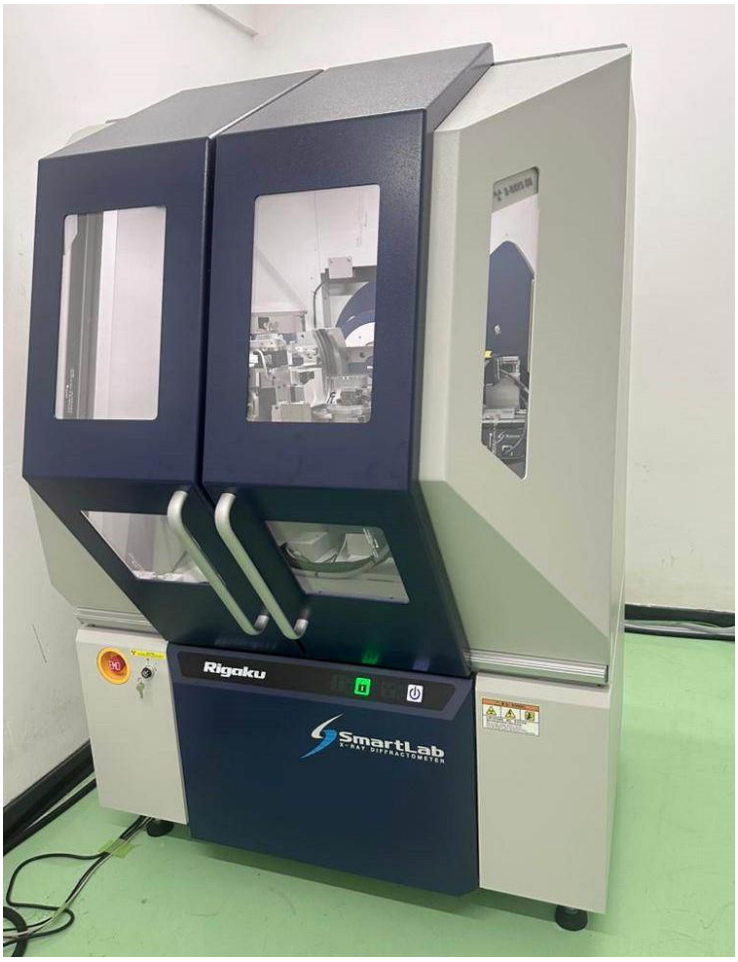

Figure II. 9 Rigaku SmartLab Diffractometer

II.2.1.2. Raman spectroscopy method

The spectroscopic technique known as Raman spectroscopy based on the inelastic scattering of monochromatic light, typically from a laser source. When monochromatic light interacts with a sample, inelastic scattering occurs, changing the frequency of the photons. The sample absorbs laser photons, which are then reemitted. The Raman Effect refers to the alteration in the frequency of emitted photons, either upwards or downwards, from the original monochromatic frequency. A laser beam in the ultraviolet (UV), visible (Vis), or near infrared (NIR) range is typically used to illuminate a sample. The Raman spectrum of a material is obtained by collecting scattered light using a lens and sending it through an interference filter or spectrophotometer. [21]

Raman spectroscopy used in the characterization is: Rapid Microcoagulation Raman Imaging System Model: **Horiba LabRam HR Evolution {China}**

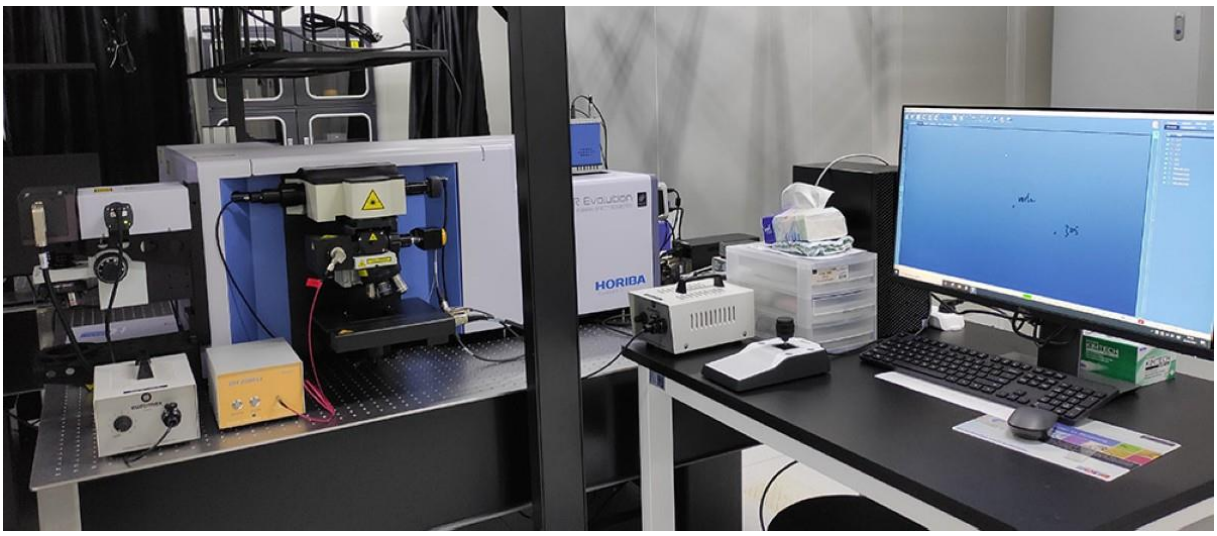

Figure II. 10 Rapid Microcoagulation Raman Imaging System

II.2.2. Optical properties

II.2.2.1. UV-Vis-NIR method

The UV-visible-NIR spectrophotometer employs photon spectroscopy within the range of 300 to 1500 nm. This method pertains to absorption spectroscopy, wherein electrons are excited from the ground state to an excited state. Conversely, fluorescence gauges transitions from the excited state to the ground state. The reflectance of thin films as well as a combination of the absorption coefficient and film thickness have an impact on their transparency. [58,59]

The transmittance (T) is typically related to the absorption coefficient (α) by the equation to remove the interference fringes impact: [58]

$$T \cong (1 - R)e^{-\alpha d} \qquad \text{(II.5)}$$

where: α is the absorption coefficient.
d is the thickness of the film.
T is the transmittance
R is the reflectance

The absorption coefficient (α) can be calculated using the following expression: [52]

$$\alpha = \frac{1}{d}\ln\left(\frac{100-R\%}{T\%}\right) \quad \text{(II.6)}$$

Figure below shows the principle of UV-visible-NIR spectrophotometer:

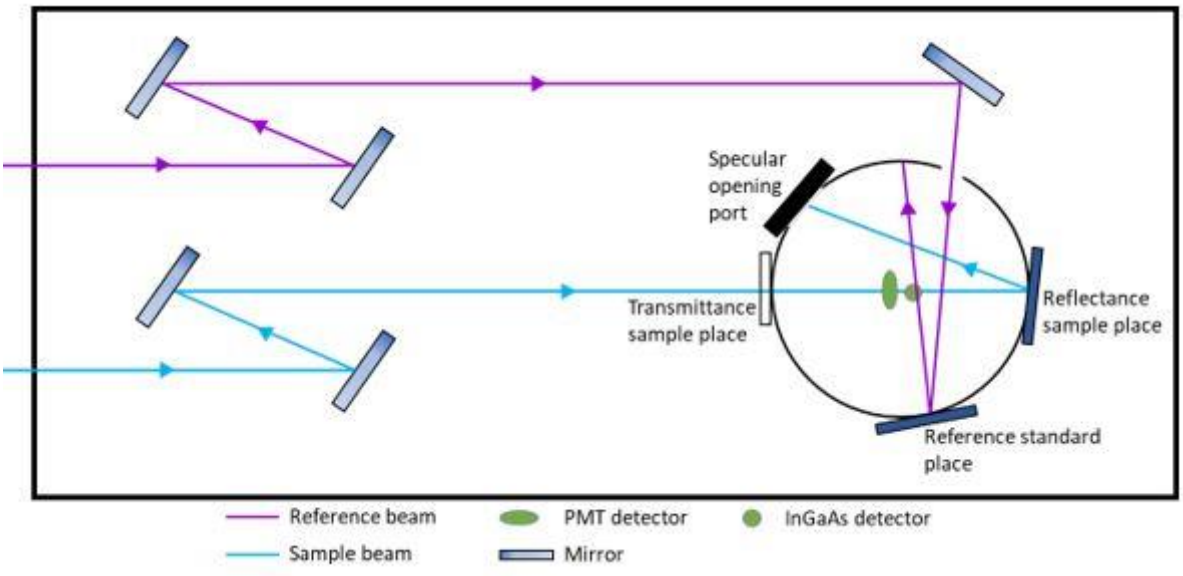

Figure II. 11 Principle of UV-visible-NIR spectrophotometer

II.2.2.1.1. Film thickness measurement by Swanepoel method

We calculate film thickness from the following equation [21,60]:

$$d = \frac{\lambda_1\lambda_2}{2(\lambda_1 n_2 - \lambda_2 n_1)} \quad \text{(II.7)}$$

Where: n_1 and n_2 are the refraction index of the film for the wavelength λ_1 and λ_2 respectively.

we can calculate n_1 and n_2 from the following relation:

$$n_{1,2} = \left(N_{1,2} + \left(N_{1,2} + S^2\right)^{\frac{1}{2}}\right)^{\frac{1}{2}} \quad \text{(II.8)}$$

Where: S is the refraction indexes of the substrate

And $N_{1,2}$ can be obtained using this relation:

$$N_{1,2} = \frac{2S(T_M - T_{m1,2})}{T_M T_m} + \frac{S^2+1}{2} \quad \text{(II.9)}$$

Where: $T_{m1,2}$ is the minimum transmittance corresponds with $\lambda 1$, $\lambda 2$ and T_M is the maximum transmittance confined between T_{m1} and T_{m2} as shown in the following figure:

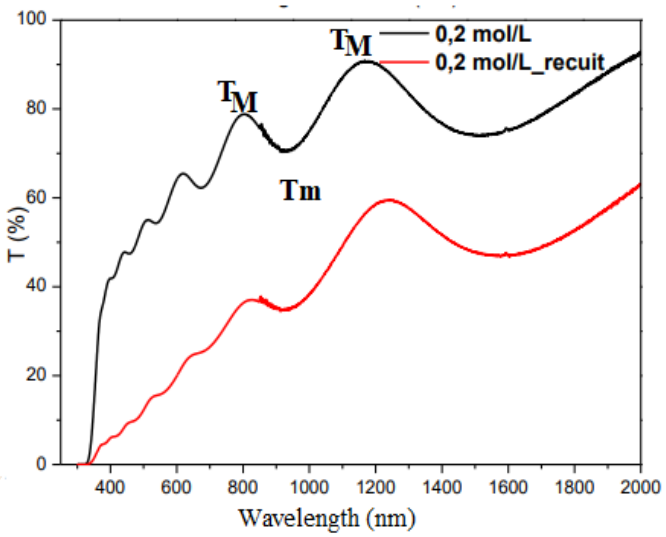

Figure II. 12 : Transmittance spectra of TiO_2 thin films obtained before and after annealing [19]

II.2.2.1.2. Optical band gap E_g

In high energy, absorption results from electronic transitions between wide states of band to band. It is usually described by Tauc law [32]:

$$(\alpha h\nu)^n = A(h\nu - E_g) \qquad \text{(II.10)}$$

Where: $h\nu$ is the photon energy.

E_g is optical band gap.

n and A are constants.

α is the absorption coefficient.

n characterizes the optical type of transition and takes the values 2, 1/2 (2 for allowed direct transitions or 1/2 for allowed indirect transitions).

From the curve of $(\alpha h\nu)^n$ as function $(h\nu)$ optical band gap was estimated by extrapolating the linear part of the plot of $(\alpha h\nu)^{1/2}$ as a function of $h\nu$ to intercept the energy axis (at $\alpha h\nu = 0$) as shown in figure below:

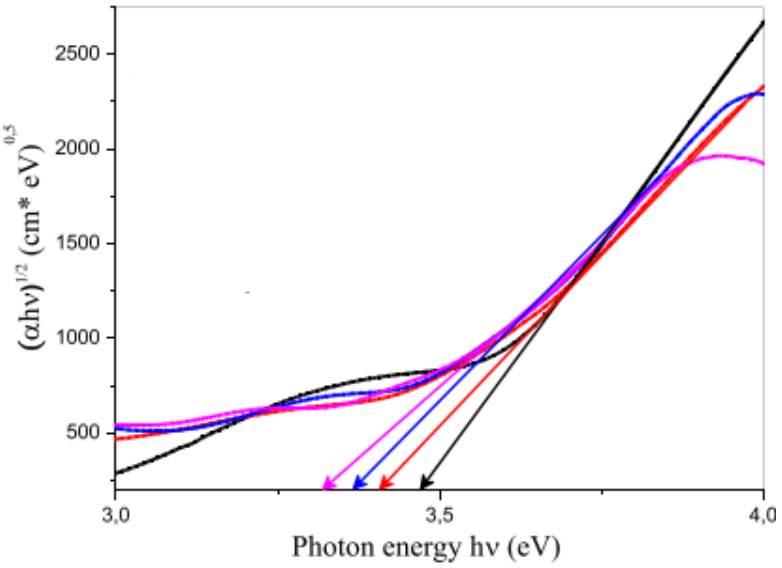

Figure II. 13 The plot of $(\alpha h\nu)^2$ versus hν of anatase TiO_2 thin films deposited on glass substrate using different precursor concentration [52]

II.2.2.1.3. Urbach energy ($\boldsymbol{E_u}$)

When in a material there are variations in interatomic distances, bond lengths or angles, what is called a "disorder (Urbach region)" appears, thus, the Urbach energy can be considered a parameter that includes all possible defects. The relation between the Urbach energy and absorption coefficient is described by [21,59]:

$$\alpha = \alpha_0 \exp\left(\frac{h\nu}{E_u}\right) \quad \text{(II.11)}$$

Where: α_0 is a constant and E_u is Urbach energy.

By drawing $\ln(\alpha)$ versus $h\nu$ we can determine E_u value as the reciprocal of the linear part slope (Figure II.14):

$$\ln(\alpha) = \ln(\alpha_0) + \frac{h\nu}{E_u} \quad \text{(II.12)}$$

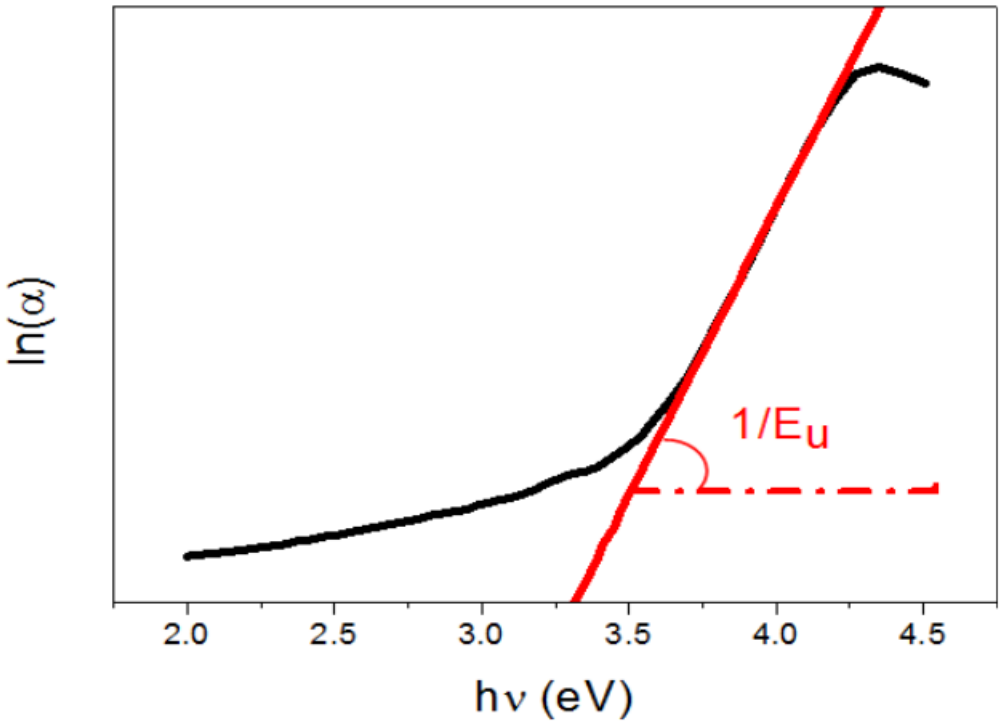

Figure II. 14 Determination of Urbach energy E_u

Optical characterization was determined by: UV-Vis-NIR Absorption Spectrometer Model: **HITACHI UH4150 {China}**

Figure II. 15 UV-Vis-NIR Spectrophotometer

II.2.3. Morphological properties

II.2.3.1. Field Emission Scanning electron microscope method

The Field Emission Scanning Electron Microscope (FESEM) is a type of electron microscope that images the sample surface by scanning it with a high-energy beam of electrons in a raster scan pattern. The electrons interact with the atoms to make the sample producing signals that contain information about the surface of the sample, composition and other properties of thin films.

As shown in figure II.16, the FESEM uses electrons instead of light to form an image. A beam of electrons is produced at the top of the microscope by heating of a metallic filament. The electron beam follows a vertical path through the column of the microscope. It makes its way through electromagnetic lenses which focus and direct the beam down towards the sample. Once it hits the sample, other electrons such as backscattered or secondary are ejected from the sample. [34]

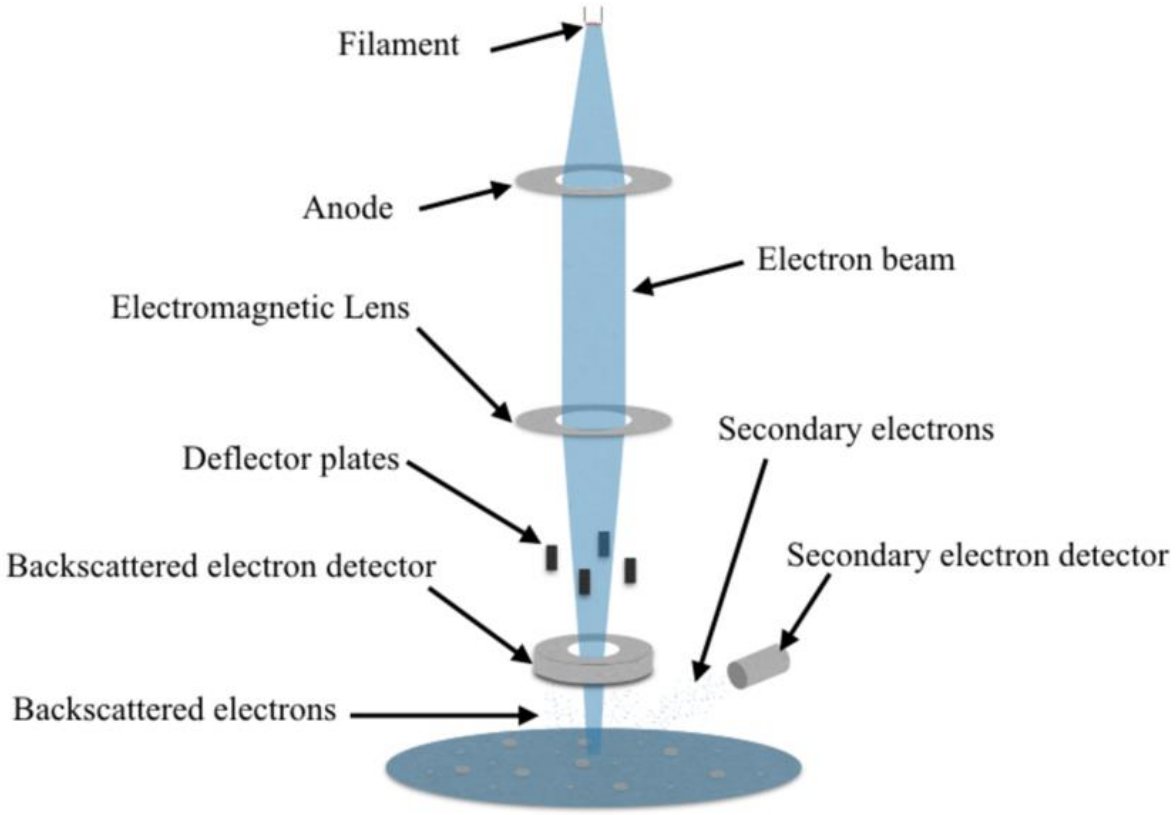

Figure II. 16 Field Emission Schematic of Scanning electron microscope (FESEM)

Results of FESEM was obtained by Field Emission Scanning Electron Microscopy Model: **Gemini 300 {China}**

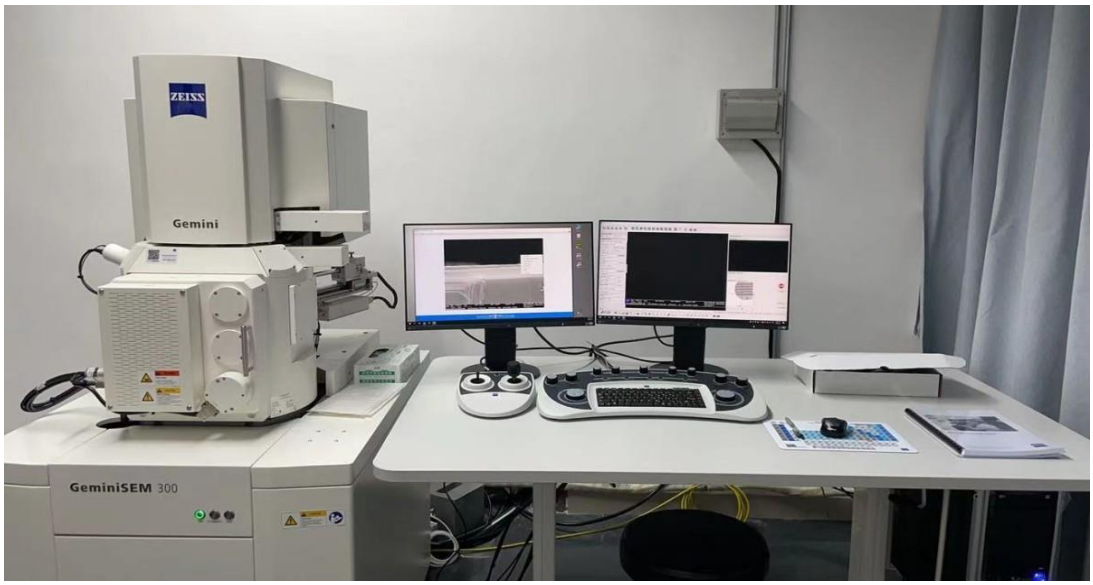

Figure II. 17 Field Emission Scanning electron microscope (FESEM)

II.2.4. Attenuated Total Reflectance Fourier Transform Infrared (ATR-FTIR) spectroscopic method

One of the main sampling methods used in Fourier transform infrared spectroscopy (FTIR) to study the surface of materials properties is attenuated total reflectance-FTIR (ATR-FTIR). An ATR crystal having a high refractive index, such as germanium, is positioned beneath the sample in ATR-FTIR, as depicted in Figure II.18. Total internal reflection occurs when IR radiation strikes the crystal, and the resulting evanescent waves are absorbed by the sample. For a reliable ATR-FTIR spectrum, good contact between ATR crystal and test sample is required due to typically low penetration depth of the evanescent waves. [61]

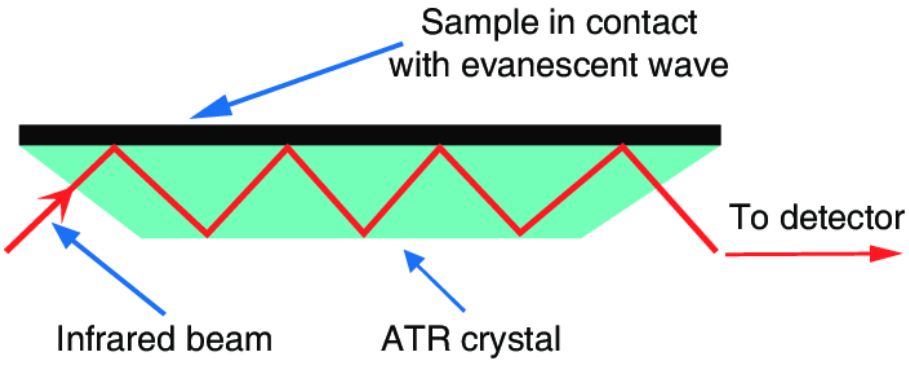

Figure II. 18 Schematic of ATR-FTIR measurement principle

ATR-FTIR device used in the measurements is: Attenuated Total Reflectance Fourier transform infrared spectrometer Model: **INVENIO-R {China}**

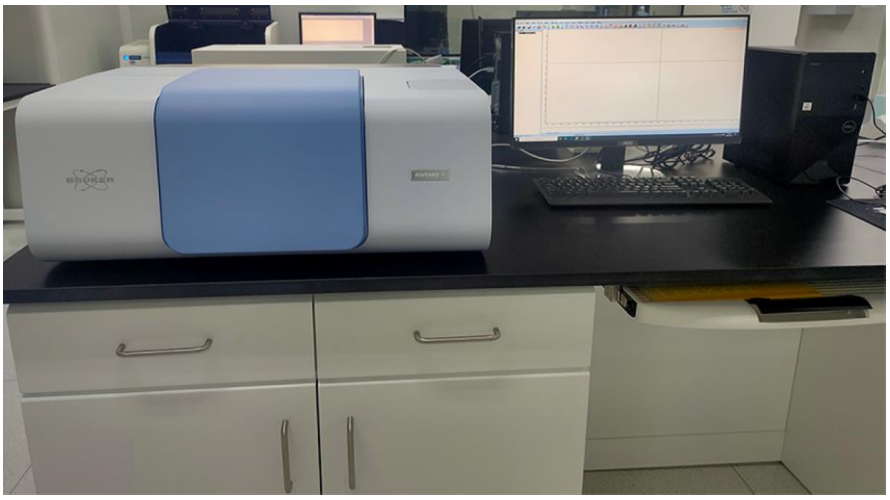

Figure II. 19 Fourier transform infrared spectrometer

II.2.5. Photoluminescence PL method

photoluminescence (PL) spectroscopy technique uses to investigate the structure, defects, impurity levels and quality of thin films. Through PL measurement, we can obtain a variety of material parameters, which will be introduced respectively as follows [34,56]:

- Band gap energy.
- Impurity levels and defects detection.
- Recombination mechanisms.
- Material quality.

PL device used in this study is: Fluorescence Spectrometer Model: **HITACHI F-7100 {China}**

Figure II. 20 Fluorescence Spectrometer

Chapter 3 :

Preparation, structural, and morphological characterizations of TiO_2 thin films

In this chapter, we will discuss the steps of preparing our thin films of titanium dioxide (TiO_2) using the ultrasonic spray deposition technique. The structural, and morphological characterizations of the samples prepared by several ways, namely: X-Rays diffraction, Raman spectroscopy, Field Emission Scanning Electron Microscopy FESEM, ATR-FTIR. This study allows us to know the general properties of titanium dioxide: the structural and morphological properties.

III.1. Experimental procedures

III.1.1. Choice of deposition substrate

The TiO_2 thin films studied are deposited on glass slides because of: [19,62]

- its good thermal expansion agreement with TiO_2 to reduce the impacts of substrate/material tensions during deposition.
- its transparency, which is ideally suited for the optical characterizations of the films in the visible spectrum.
- available and less expensive.

III.1.2. Cleaning of the substrates

The process for cleaning the substrates is as follows:

- Rinse with distilled water.
- Cleaning with acetone for 5 min to remove grease.
- Rinse with distilled water for 5 min.
- Cleaning with alcohol for 5 min.
- Rinse with distilled water for 5 min.
- Drying.

Cleaning the substrates is an essential step that must be completed in a clean environment since it determines the adherence and homogeneity of the thin films that is being deposited.

III.1.3. Preparation of the solutions

In all the samples, the main spray solution which contains the titanium tetra-isopropoxide solution ($Ti[OCH(CH_3)_2]_4$) was utilized as a precursor, ethanol [C_2H_5OH] as a solvent, and acetylacetone [CH_3COCH] as a catalyst. TTIP and acetylacetone have a molar ratio of 1:2.

The properties of elements used in solution are mentioned in tables below:

Table III. 1 Element properties of solution

	Precursor ($Ti[OCH(CH_3)_2]_4$)	**Solvent (C_2H_5OH)**	**Catalyst (CH_3COCH)**
physical state	Liquide	Liquide	Liquide
Color	Transparent	Transparent	Transparent
The purity	95	absolute	99.5
Density g/cm^3	0.955	0.789	0.97
molar mass g/mol	284.25	46.07	100.12

III.1.4. Experimental conditions

The PH of the solution is the variable parameter in our work on the thin films deposition of titanium dioxide (**PH=2.5 ; PH=6.5 ; PH=10.5)** , and the experimental conditions of the elaborations of our TiO_2 thin films represented in the following table :

Table III. 2 Experimental conditions of the deposition serie

The settings		**Reference**
Nozzle-substrate distance	5 Cm	[40,52]
The substrate temperature	450 °C	[62,63]
The deposition time	2 min	[52]
Solution flow rate	50 ml/h	[34,40,41]

III.2. Thin films deposition procedure

When the substrates and the solutions are ready, we begin to deposit our samples. First, we put the solution in the syringe and attach it to the syringe pump. Next, we place the substrate on top of the heating plate of the ultrasonic spray device, which is attached to a temperature controller set to 450° C. The flow rate of the solution is at 50 ml/h. Very fine droplets about 40 µm of size are sprayed onto the heated substrate. This allows the activation of the chemical reactions between the compounds and the formation of our thin films start.

III.3. The effect of PH

III.3.1. Preparation of solutions

Among the parameters used to change the properties of thin films of titanium dioxide using an ultrasonic spray pyrolysis is the PH. We prepared three solutions from the chemical elements (table III.1), the main simple solution (without additions, PH=6.5), and we prepared two additional solutions, so that HCl was added to the one of the solution (PH=2.5) and the NH_3 to the second solution (PH=10.5), so that we had 3 solutions with three different PH measured by PH-meter (PH=2.5 , PH=6.5 , PH=10.5).

Following figure describe the experimental procedure for the different PH solution:

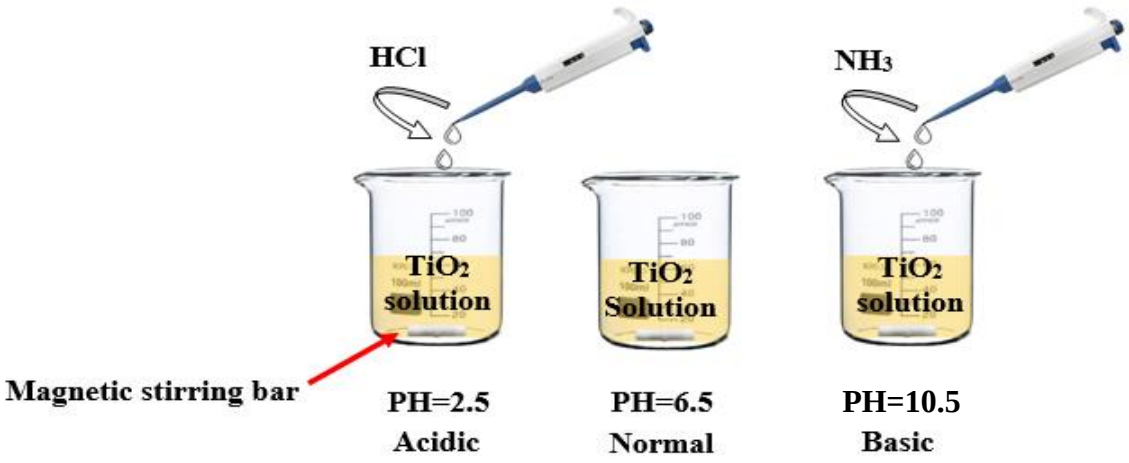

Figure III. 1 Experimental procedure for the preparation of different PH solution

III.4. The effect of annealing

According to technological requirements, annealing is employed to enhance the physico-chemical properties of thin films. Annealing can be done for a period of time at a specific temperature in air, a vacuum, or a gas environment, followed by typically slow cooling. This process enhances the crystallization of films and some of its physical properties. [19]

For our samples, we did a heating process at 600°C for 2 hours to improve the crystallization of the TiO_2 films and some its physical properties.

The steps of practical work are brief and shown in figure below:

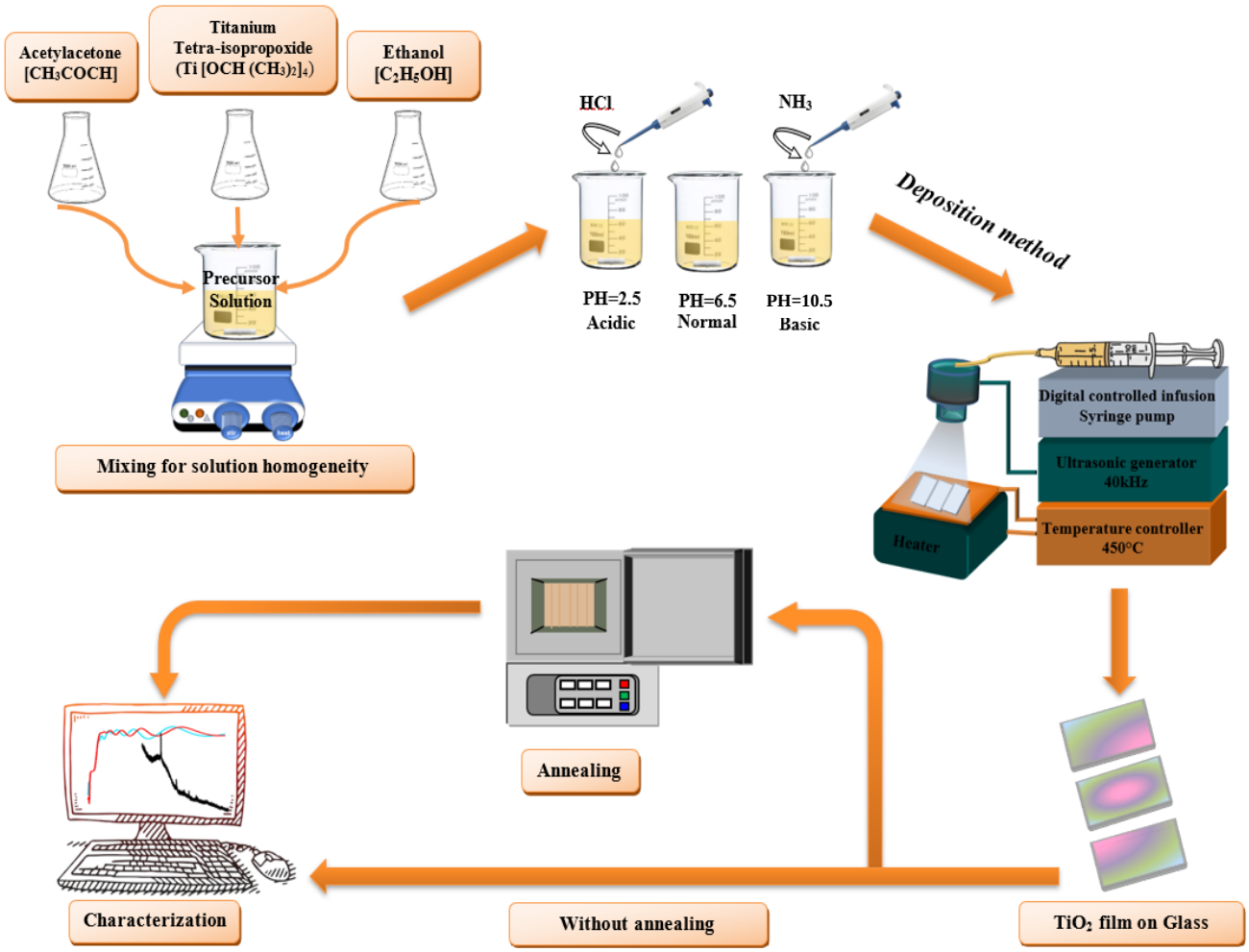

Figure III. 2 Schematic of practical work

III.5. Adhesion test

The adhesion strength between deposited thin films and their substrates can be evaluated in a variety of ways. This test frequently happens before applying any characterization, and in this study, it was specifically evaluated on the thin films applied with Scotch adhesive tape. The degree of adherence is considered "good" if the thin film adheres to the substrate (figure III.3)

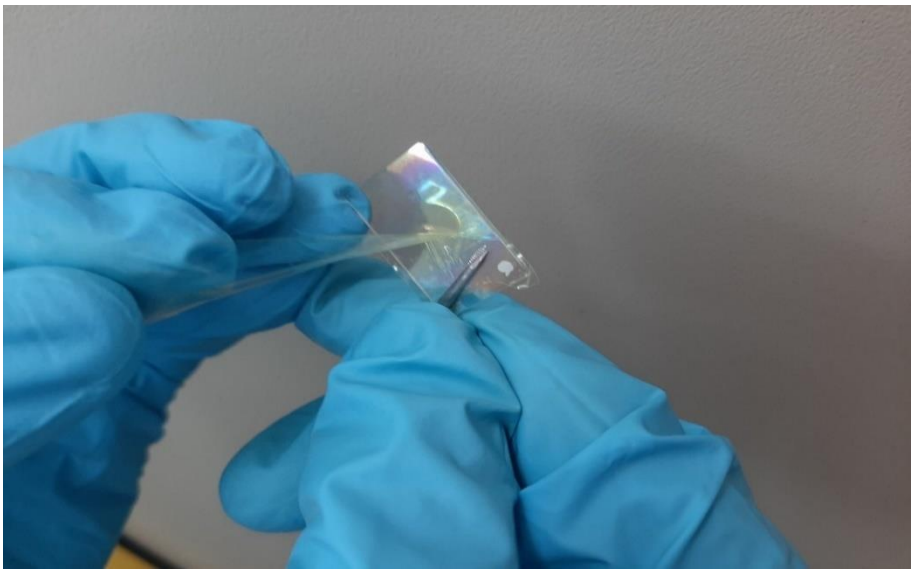

Figure III. 3 Simple adhesive tape test for our TiO_2 thin films

III.6. Characterizations of TiO_2 thin films

III.6.1. Thickness of thin films

We can obtain thickness of our elaborated TiO_2 thin films using the Field Emission Scanning Electron Microscopy FESEM **Gemini 300**, we obtain the cross sectional of thin films which are elaborated at PH=10.5 before and after the annealing at 600°C (figure III.4).

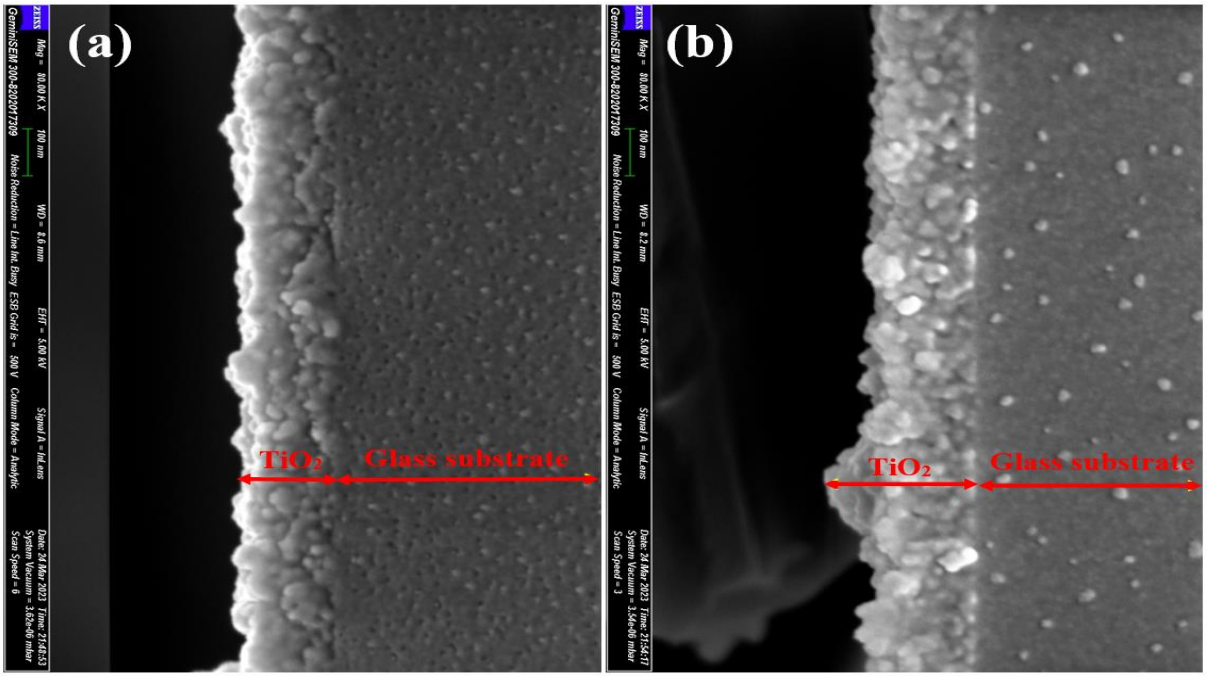

Figure III. 4 Cross sectional by FESEM
(a) cross sectional before annealing , (b) cross sectional after annealing

The results of the thickness measurements by the cross-sectional method were close to the results of Swanepoel method shown in the table III.4, and therefore we choose to work with the results of Swanepoel method.

We can determine thickness also from Swanepoel method (equation II.7 mentioned in chapter II). The variation in thickness is summarized according to PH precursor values of solution used before and after the annealing in the following table:

Table III. 3 The variation of thickness with different values of PH precursor solution with and without annealing

PH of solution	Thickness of thin film (nm)	
	Before annealing	After annealing
PH=2.5	472	431
PH=6.5	749	653
PH=10.5	308	243

III.6.2. Growth rate of thin films

The growth rate of our thin films was calculated from the thickness (obtained from Swanepoel method) division over the deposition time. The growth rate values of our TiO_2 thin films are presented in the following table:

Table III. 4 Growth rate of TiO_2 thin film in different PH precursor solution values

PH of solution	Rate of growth (nm/min)	
	Before annealing	After annealing
PH=2.5	236	215.5
PH=6.5	374.5	326.5
PH=10.5	154	121.5

The variation of the growth rate and the thickness of TiO_2 as a function of the PH precursor solution values before and after annealing is presented in table III.3, III.4 and figure III.5 (a,b). Before the annealing (figure III.5a) we observe that the PH of solution at 6.5 has the largest value of thickness estimated at 749 nm, at PH=2.5, the thickness decreases to 472 nm. The lowest value for thickness is at a basic PH=10.5 and is estimated at 308 nm. We observe the same evolution in growth rate values. This results when the PH rises (basic medium), more OH^- ions enter the solution and they have a tendency to interact easily with titanium atoms, leaving insufficient titanium for TiO_2 to develop on the substrate. Hence, the chemical reactions to produce the nuclei onto the substrate decreases. This conclusion is also indicated by thickness measurements which show a thinner layer at increased PH (10.5). [64]

Figure below (III.5) show the variation of thickness and growth rate as a function of PH precursor solution values, before and after annealing.

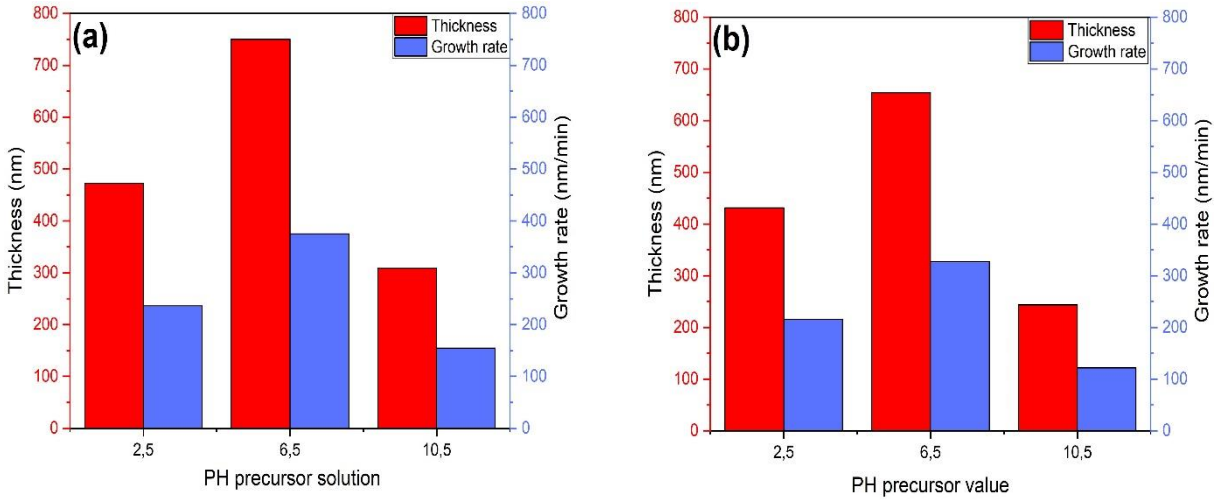

Figure III. 5 Film thickness and growth rate variation of our thin films depending on PH precursor solution value
(a) before annealing , (b) after annealing

After annealing **(**figure III.4b), we observe the same evolution for both thickness and growth rate. We notice that the thickness and growth rate of our thin films decrease with annealing. The greatest value of thickness is predicted to be 653 nm at a PH=6.5, while at PH=2.5, the thickness decreases to 431 nm. The lowest value for thickness is at a basic medium PH=10.5 and is estimated at 243 nm. This decrease can be explained by the effect of annealing as follows: the decrease could be originated by the increment of material density owing to the evaporation of organic residual coming from the precursor solution [59]

III.6.3. Structural characterization by XRD (X-rays diffraction)

The crystallization phase of the prepared thin films was investigated with the effect of PH before and after the annealing, using the X-ray diffraction technique (chapter II) using a type of **Rigaku SmartLab Diffractometer**, of configuration 2θ-θ and having a CuK_α radiation source of wavelength λ = 1.540593 Å.

The XRD spectra of TiO_2 thin films deposited at different PH precursor values before and after annealing are shown in Figure III.6 (a,b).

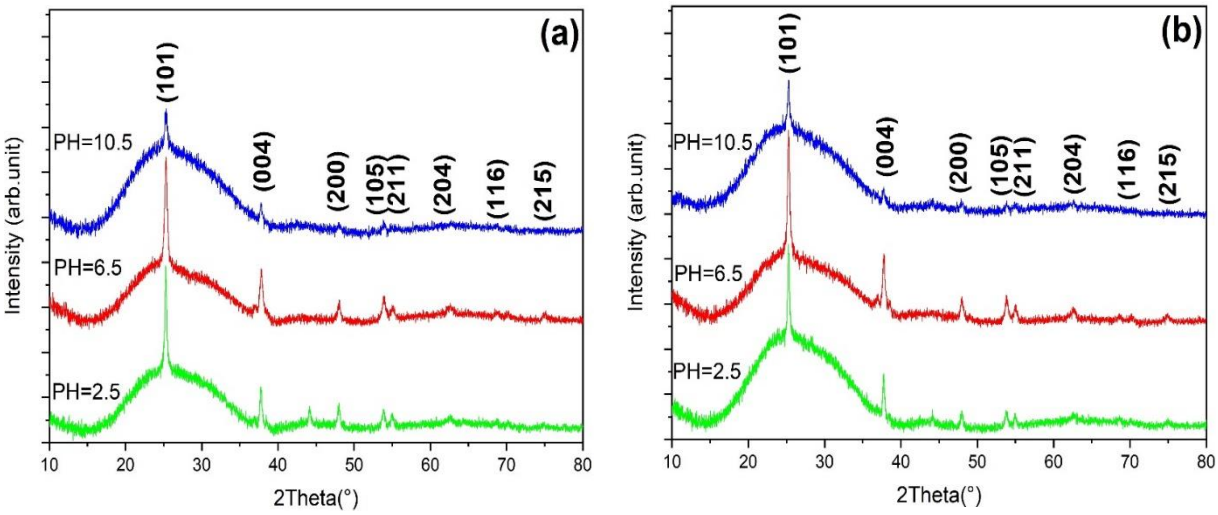

Figure III. 6 The X-ray diffraction spectra of our TiO_2 thin films
(a) before annealing , (b) after annealing

We observe for both before and after annealing, the presence of planes (101), (004), (200), (105), (211), (204), (116), (215), corresponding to the diffraction angles of 25.23°, 37.87°, 47.98°, 53.80°, 55.13°, 62.54°, 68.76°, 75.14° respectively. These planes point to the anatase phase and the presence of these orientations in X-ray spectra indicates that the films are polycrystalline. The crystal structure of this phase is tetragonal with lattice parameters: a=b=3.782 Å and c =9.430 Å, and are in good agreement with reported data (ICCD N° 21-1272, see annex). On the other hand, it is important to note that there is a preferential growth orientation of the TiO_2 crystallites according to the (101) plane, which is logical due to the small formation energy of this plane according to another plane [21]. It should be noted that before annealing the intensity of the X-ray diffraction peaks in the case of PH=6.5 is very large indicating a high degree of crystallinity, this is explained by an increase in nucleation sites brought on by more material being deposited on the surface of substrate [65], but for the case of PH=10.5 the intensity of the peaks becomes very weak and broader. After annealing It can be seen that we have the same peaks planes, we observe the increase in the intensity of the peaks due to annealing temperature. The change appears clearly in thin films deposited at

PH=6.5, and lowest variation is at PH=10.5, this phenomenon is related with research of V. Gopala Krishnan et .al [66]

III.6.3.1. Crystallite size D and dislocation density δ

By exploiting the equations (II.2 and II.3) mentioned in chapter II, we determined the crystallite size and the dislocation density of our TiO_2 thin films for the most intense peak (101) for anatase, the results are summarized in the following tables:

Table III. 5 The crystallite size of our TiO_2 thin films

PH precursor solution	Crystallite size " D " (nm)	
	Before annealing	After annealing
PH=2.5	28.56	29.86
PH=6.5	20.09	24.09
PH=10.5	22.34	27.37

Table III. 6 The dislocation density of our TiO_2 thin films

PH solution	Dislocation density " δ "(10^{14} line /m^3)	
	Before annealing	After annealing
PH=2.5	12.26	11.22
PH=6.5	24.77	17.23
PH=10.5	20.04	13.35

As can be seen in Table III.5, III.6 and the figure below (figure III.7), the crystallite size and dislocation density are affected by the PH. So we find before annealing that the highest value of the crystallite size is at the PH of the acidic medium (PH=2.5), while the lowest value was in the normal medium (PH=6.5) , This behavior can be explained on the basis of the fact that for low PH values (PH=2.5), the low-hydrolyzed species will exhibit a high condensation velocity, which means that the process of thin film growth is enhanced, favoring the formation of big crystallite size. These results suggest that the structural properties of the films are enhanced with solution acidity and may be attributed to the increase in the crystallite

size [67]. Our results are in agreement with the work of Ouissem Chibani et al, and Siti Aida Ibrahim et al [67,68].

Concerning dislocation density, we notice the opposite behavior of the crystallite size, the highest value of dislocation density is in the normal medium (PH=6.5), and the lowest is for the acidic medium (PH=2.5). This decrease was caused by the increase in the crystallite size because when the size of the crystals increases, the joints will automatically decrease [19]. This result can be confirmed by the crystallite size variation.

After the annealing, we notice an increase in crystallite size and decrease in dislocation density with the same variation like before annealing. This can be explained by: the recrystallization of the quantity of the material which was not yet crystallized before annealing, means that which means improving the crystalline state of films due to the raise of nucleation centers after annealing treatment [21], in addition may be explain this evolution in crystal structure that the energy is sufficient.

Following figure present the evolution of Crystallites size, dislocation density before and after annealing:

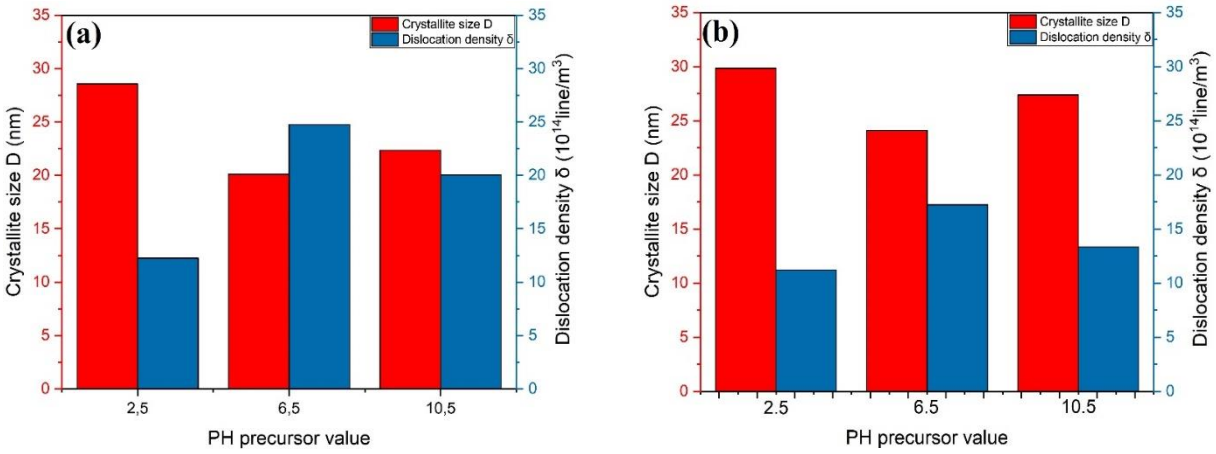

Figure III. 7 The evolution of Crystallite size D, dislocation density δ
(a) before annealing , (b) after annealing

III.6.3.2. Micro-Strain (ε)

The results of the micro-strain of TiO_2 thin films are shown in Table III.7:

Table III. 7 The micro-strain of our TiO_2 thin films

PH precursor solution	Micro-Strain " ε " (10^{-3})	
	Before annealing	After annealing
PH=2.5	5.55	5.31
PH=6.5	7.88	6.57
PH=10.5	7.08	5.79

The table III.7 and figure III.8 present the variation of micro-strain of our thin films according to PH precursor values. It can be seen that before annealing, the thin film deposited at PH=6.5 is characterized by a large deformation compared to the other films. It can explain these results by the variation in crystallite size, when it increases, micro-strain decreases due to reduction in defect density inside the films [34]

We notice that the annealing affects the deformation of our thin films. After annealing, the thin films deposited are characterized by a small deformation, which means that micro-strain decreases with annealing. This reduction in micro-strain may be due to the procedure of recrystallization of TiO_2 crystallites.

Figure below shows the variation in micro-strain before and after annealing:

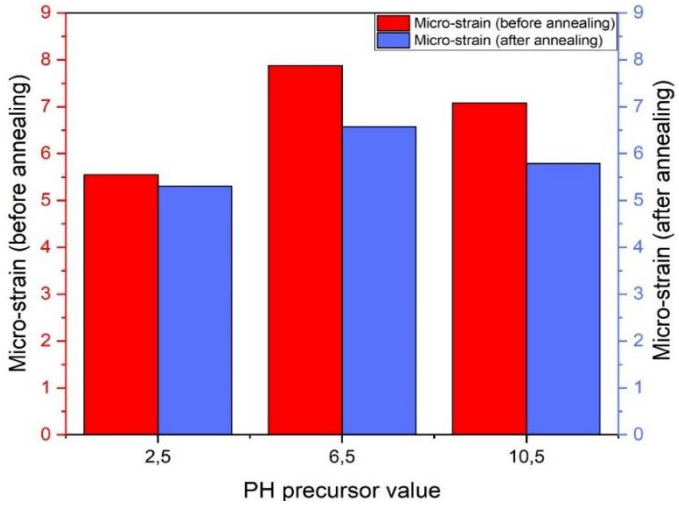

Figure III. 8 The variation in micro-strain before and after annealing.

III.6.4. Raman spectroscopy

Raman spectroscopy has been used to investigate the chemical composition, crystallinity, structural defects, and size effect of nanoscale crystallites. In our study, Raman spectroscopy used in the characterization is : Rapid Microcoagulation Raman Imaging System Model: **Horiba LabRam HR Evolution** (mentioned in chapter 2).

Figure III.9 shows the Raman spectra of our samples in different PH precursor values before and after annealing (at 600°C):

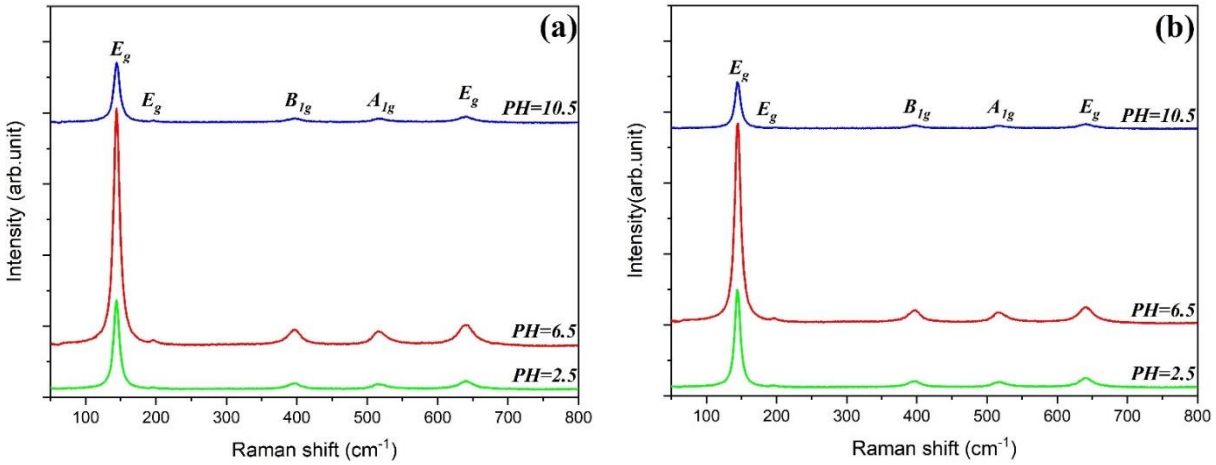

Figure III. 9 The Raman spectra of our TiO_2 thin films elaborated at different PH precursor values
(a) before annealing , (b) after annealing

As seen in figure III.9, laser Raman microspectroscopy indicates the presence of anatase phase in all of the films, with bonds 144, 195, 397, 514, and 638, refer to $E_{g(1)}$,$E_{g(2)}$, B_{1g}, A_{1g}, and $E_{g(3)}$ respectively [69].

We can observe that the effect of PH precursor is clear in our Raman spectra for our samples. The highest intense peak at in PH=6.5, and lower intense peak is in basic medium (PH=10.5), this indicates a best crystallinity means that high crystallite density at PH=6.5 , which is confirmed by the XRD results.

We notice that the annealing temperature affect the intense of our peak, and that was explained in XRD results (recrystallization of thin films).

III.6.5. Field Emission Scanning Electron Microscopy FESEM

The surface morphology of the films were examined by Field Emission Scanning Electron Microscopy FESEM Model: **Gemini 300**.

Figure III.11 illustrates the morphology of our TiO_2 thin films. All the films clearly show a homogeneous, smoothing surface, and uniform grain size, without cracks, and pinholes in various PH precursor values before and after annealing (see figure III.11), indicating that the films are well adherent to the substrates. [59,70]

We can notice that at high Value of PH precursor (PH=10.5), we have a tiny granular particle. When PH precursor decreases (PH=2.5), the surface of the films becomes more uniform as shown in cross sectional figure (III.10), with the larger grain size indicating an increase in crystallinity. According to FESEM results, the grain size varies depending on the PH precursor of solution, which is in accordance with structural study (XRD measurement). [66]

Cross sectional image (figure III.10), confirm the variation in grain size with PH precursor value:

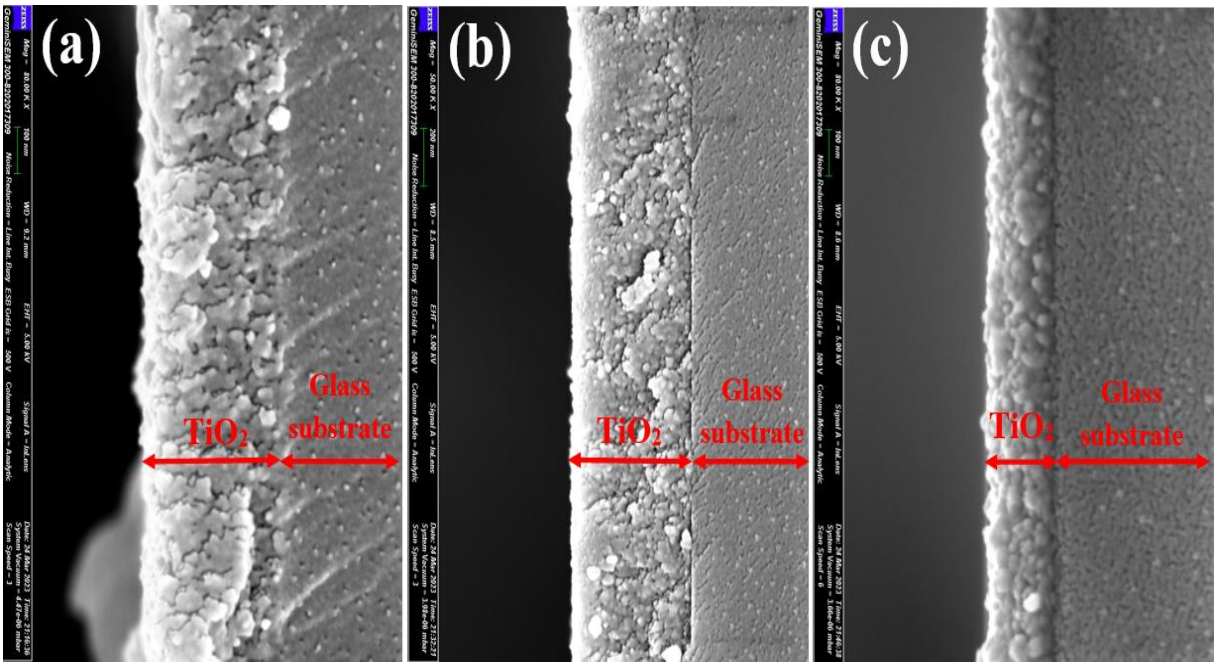

Figure III. 10 Cross sectional image obtained by FESEM in different PH precursor values (a) PH=2.5 , (b) PH=6.5 , (c) PH=10.5 (before annealing)

Figure III.11 shows FESEM images of our samples at 500, and 100 nm:

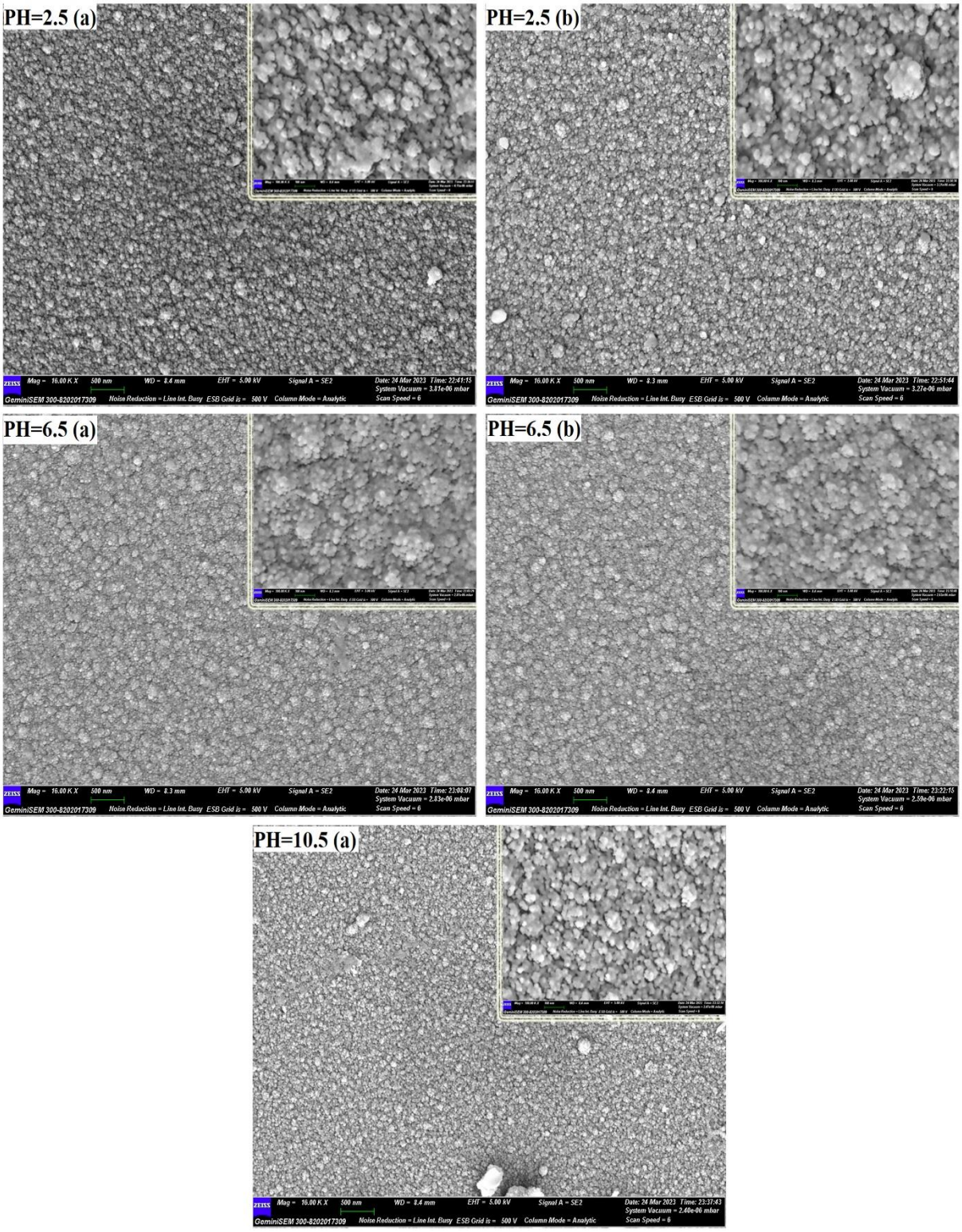

Figure III. 11 FESEM surface images of our TiO_2 thin films at different PH precursor values (a) before annealing , (b) after annealing

III.6.6. Attenuated Total Reflectance Fourier Transform Infrared (ATR-FTIR)

The ATR-FTIR characterization of our TiO_2 thin films was made by: Fourier transform infrared spectrometer **Model**: **INVENIO-R**

The ATR-FTIR spectra of our uncoated and coated glass substrates by TiO_2 elaborated in different PH precursor values by the ultrasonic spray pyrolysis technique before annealing are presented in the Figure III.12. The appearance of many transmittance peaks in the spectrum that are attributable to the vibrational modes of TiO_2 demonstrates that it has been formed. The ATR-FTIR spectra shows the presence of a significant band at around 900 cm^{-1} associated with the symmetric stretching of pure SiO_2 (Si-O-Si bonds) was seen in the control of glass sample. When TiO_2 was deposited over the glass substrate, the strength of the Si-O-Si bonds was found to decrease and a shift towards lower frequencies was noticed. This shift can be associated to the existence of Si–O–Ti and Ti-O-Si bonds, which confirm the strong adhesion between the glass substrate and the TiO_2 film [52,71]. The ATR FTIR spectra of the sample deposited at PH=6.5 demonstrate a peak in the range of 3200–3600 cm^{-1} which are related to the O–H stretching vibrations. The O–H groups are originated from the adsorption of H_2O molecules onto the surfaces of metal oxide materials. The presence of the transmittance peaks Ti-O-Ti confirm the successful formation of TiO_2 [71,72]. All the samples show some peaks at 1600 cm^{-1}, which are attributed to COO stretching vibration.

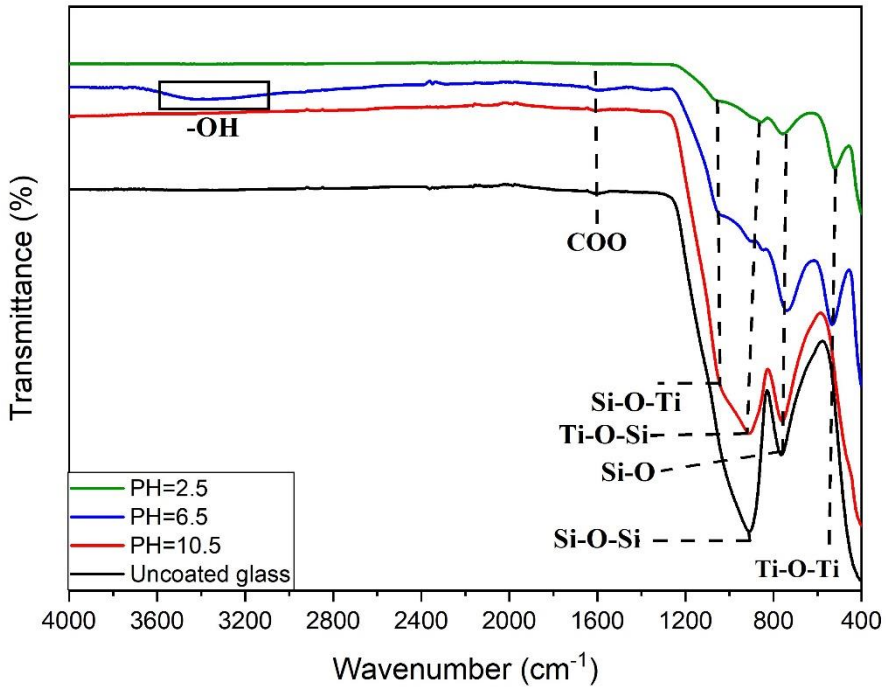

Figure III. 12 ATR-FTIR spectra of our TiO_2 thin films in different PH precursor values

Chapter 4 :

Optical Characterizations and photocatalytic application of TiO_2 thin films

This chapter is dedicated to discussing the results of optical characterizations by UV-Vis-NIR, and photoluminescence spectrophotometer, followed by the photocatalytic application of our TiO_2 thin films and their measurement.

IV.1. Optical characterizations

IV.1.1. UV-Vis-NIR spectroscopy

IV.1.1.1. Transmittance and reflectance spectra

The optical characterization of our TiO_2 thin films was made by UV-visible-NIR spectroscopy Model: **HITACHI UH4150** (mentioned in chapter II), in wavelength spectral range from 300 up to 1500 nm. The transmittance and reflectance spectra of our TiO_2 films as a function of PH precursor solution, developed before and after annealing at 600°C are shown in Figures below:

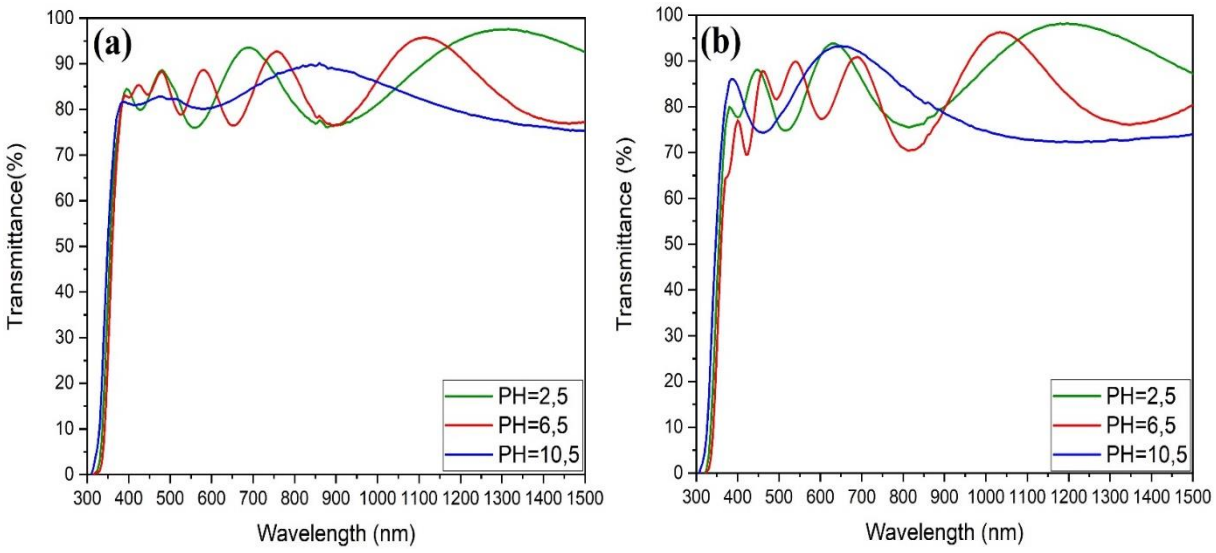

Figure IV. 1 Transmittance spectra of our TiO_2 thin films elaborated in different PH precursor values
(a) before annealing , (b) after annealing

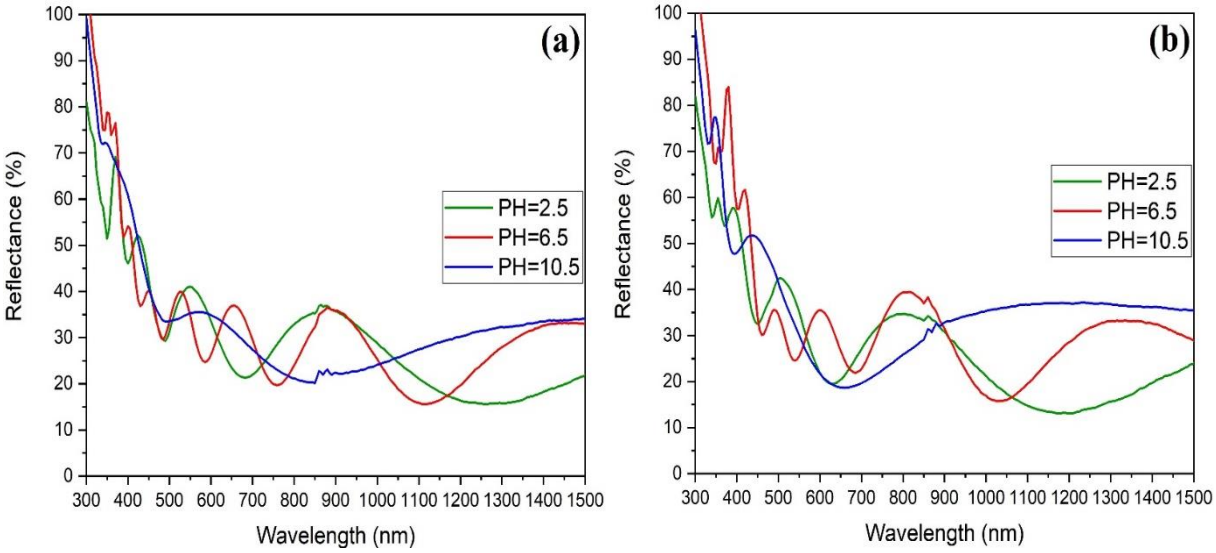

Figure IV. 2 Reflectance of our TiO_2 thin films elaborated in different PH precursor values (a) before annealing , (b) after annealing

In the wavelength range of 300–1500 nm, the figure IV.1 shows the optical transmittance spectra of our TiO_2 thin films produced from TiO_2 solutions with various PH values as-deposited and annealed at 600 °C. The elaborated films made from the solutions synthesized at PH levels of 2.5, 6.5, and 10.5 are discovered to exhibit high average optical transmittance in the visible spectral range (approximately 85 %). The oscillation transmittance may be due to the well-crystallization of film and this oscillating nature is caused due to the interference between the reflection film and substrate. Additionally, it attests to the strong adhesion on transparent glass surfaces (see cross sectional FESEM image III.10, and ATR-FTIR peaks). [66, 67]

The figure IV.3 shows the variation in the transmittance of our samples.

we can observe that all the samples have a smoothing surface, which noted in FESEM images too (figure III.11). The average of transmittance after annealing decreased by value of 2%. Thickness measurement also confirmed by the fringes (number and amplitude of transmittance waves) of the transmittance spectra.

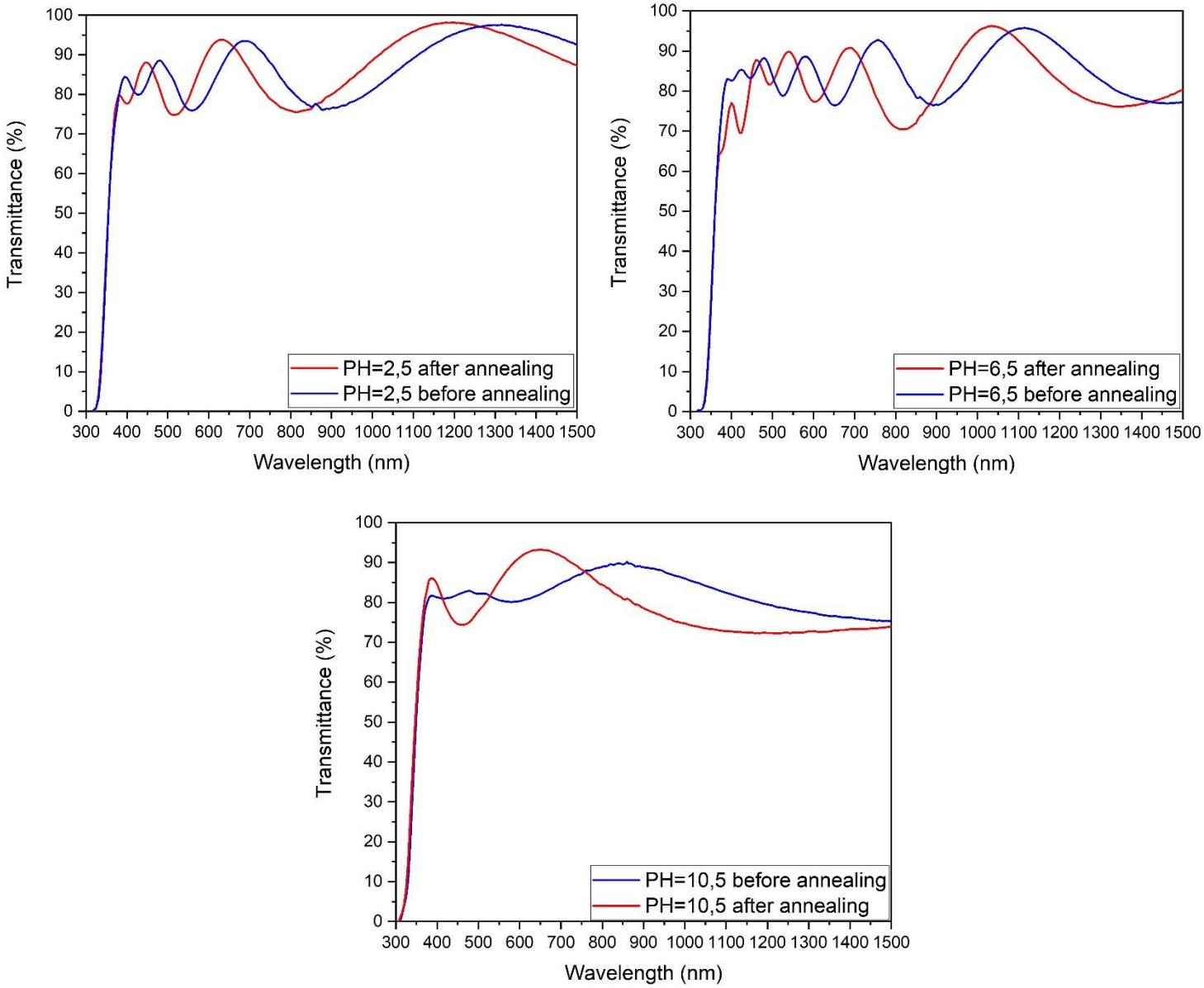

Figure IV. 3 Transmittance spectra of our TiO_2 thin films obtained before and after annealing with different PH precursor solution values

IV.1.1.2. Gap energy Eg and Urbach energy E_u (disorder)

From the transmittance spectra, the indirect Eg optical gaps and Urbach energy E_u for the TiO_2 films were deduced according to the method described in chapter II.

Following tables IV.1, IV.2 summarize the variation of Eg and E_u respectively:

Table IV. 1 Variation in indirect Eg optical gaps of our TiO_2 thin films

PH solution	Indirect Eg optical gaps (eV)	
	Before annealing	After annealing
PH=2.5	3.37	3.32
PH=6.5	3.30	3.33
PH=10.5	3.31	3.36

Table IV. 2 Variation in Urbach energy E_u of our TiO_2 thin films

PH solution	Urbach energy E_u (eV)	
	Before annealing	After annealing
PH=2.5	0.162	0.170
PH=6.5	0.164	0.160
PH=10.5	0.191	0.188

These variations are also illustrated in figure IV.4.

As seen in table IV.1 and figure IV.4, before annealing the acidic medium has a value of Eg=3.37 eV, then it decreases with the increase of PH precursor, at PH=6.5 the value is 3.30 eV, and at PH=10.5 is 3.31eV. The variation in optical band gap can be related to the crystalline state, at the PH=6.5 the optical band gap is closer to the bulk state of anatase TiO_2 (3.2 eV), the film with the best crystalline structure, according to the XRD pattern [64]. The band gap energy, a constant value of the materials for bulk samples, is known to vary in thin films due to particle size effect and film thickness. The decrease in the optical band gap of the films with an increase in the PH precursor solution could be attributed to the grain size enhancement, which takes place as a result of the faster rate of hydrolysis and polycondensation in the films deposited from solution with higher PH [73].

We can notice that at PH =10.5 has a high value of Urbach energy than the other mediums, this can be due to the small degree of crystallinity in this samples [62].

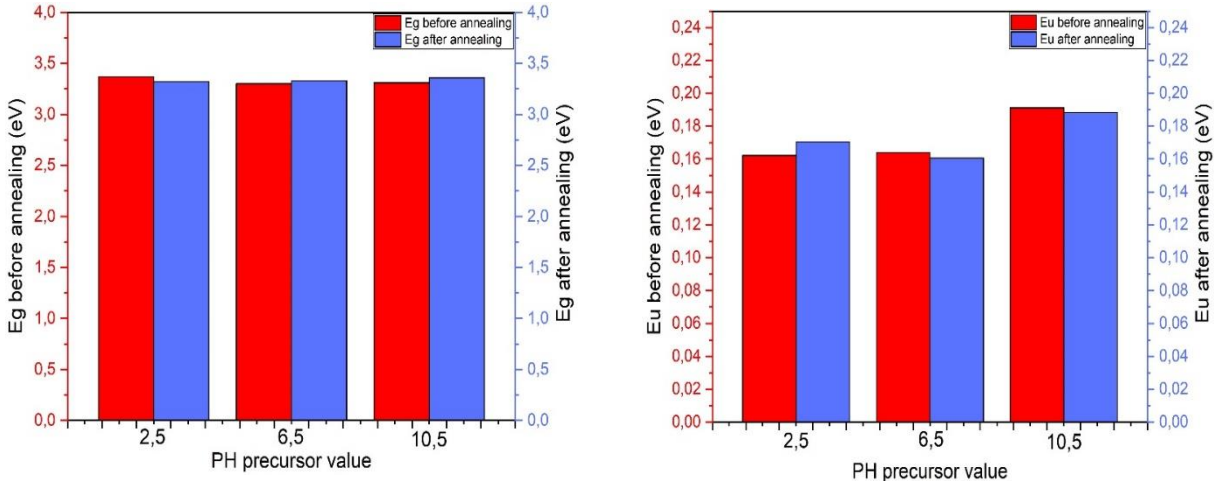

Figure IV. 4 Variations of the gap energy Eg and Urbach energy E_u before and after annealing

IV.1.2. Photoluminescence study

Photoluminescence (PL) spectroscopy technique uses to investigate the structure defects, impurity levels and quality of thin films [56]. The photoluminescence characterization of our TiO_2 thin films was made by: Fluorescence Spectrometer Model: **HITACHI F-7100.**

Figure IV.5 presents the photoluminescence spectrum of our TiO_2 films deposited at different PH precursor values, before and after annealing.

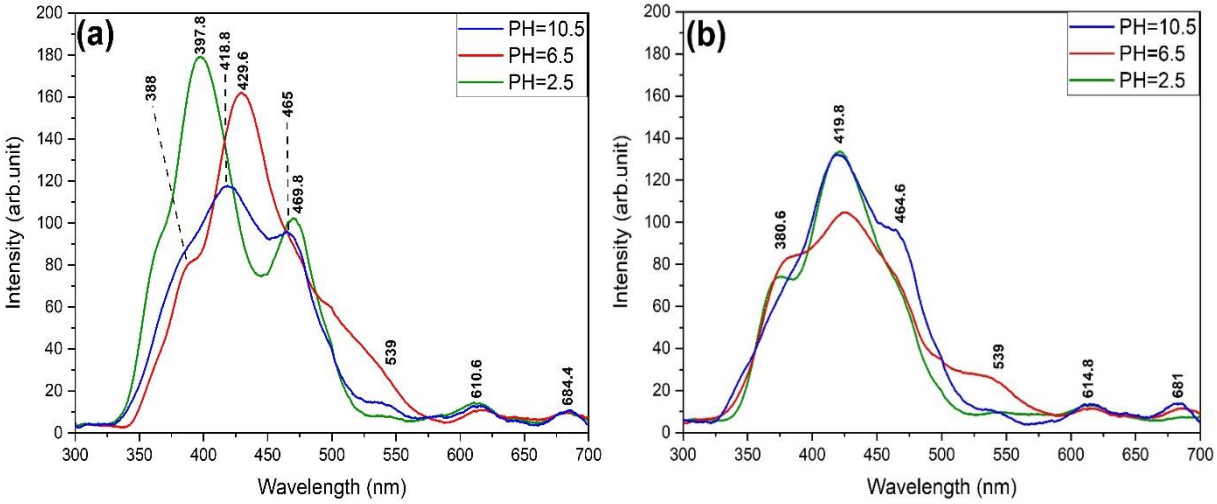

Figure IV. 5 PL spectrum of TiO_2 elaborated in different PH precursor values (a) before annealing , (b) after annealing

From figure above, we can observe that before annealing we have three interesting emission peaks. Peaks in the range of (300-500 nm) are known for the band gap energy (Eg), and the peaks between (500-700 nm) refer to the oxygen vacancies. The shift in the intense peak supports the bang gap energy Eg values. The PL spectra of TiO_2 materials is due to two types of physical sources namely surface defects, and oxygen vacancies [1,21]. It's clear from the figure above that the intensity of the peaks affected by the PH precursor. At PH=2.5 the peak has the highest intense, and this is because when the band gap contains a smaller number of defects, when the electron returns from the conduction band to the valence band, defects do not interfere with its path, which leads to the preservation of his energy, and therefore the peak is of high intensity, and this means that the intensity of the peak reflects the degree of organization in the forbidden range (Eg).

The visible emission can be attributed to the radiative defects related to the interface traps existing at the grain boundaries and which are emitted from the radiative transition between these levels and valence band. This last can be confirmed by the decrease of the peak's intensities with the decrease of the grain boundary area [1].

Through the figure IV.5, we can notice a decrease in the intensity of the peaks after annealing, and this is due to the increase in oxygen vacancies.

IV.2. Photocatalytic application

In order to test the photocatalytic activity of our elaborated TiO_2 thin films and its application to contaminant removal (water treatment), the samples were dipped in Methyl Orange (MO) solution dye and exposed to simulated solar light irradiation (UV-A) for a period of 6 hours straight.

The photocatalytic reaction is very sensitive to the catalyst surface. The reactions start when a photon with energy equal to or greater than the band gap is absorbed by TiO_2, producing an electron-hole pair that serves as the catalyst for the process [74]. The Methyl Orange reacts with radicals generated from the reactions of electron-hole pair with oxygen adsorbed and water to produce radicals, this mechanism shown in the equations written in the chapter I (from I.1 to I.8).

IV.2.1. Why did we choose Methyl Orange?

The following reasons explain why Methyl Orange molecules were selected:

- The chemical structure of Methyl Orange is stable under irradiation light. (figure IV.6)
- It is the pollutant closest to representing pollutants in nature.
- Its toxicity is very high.

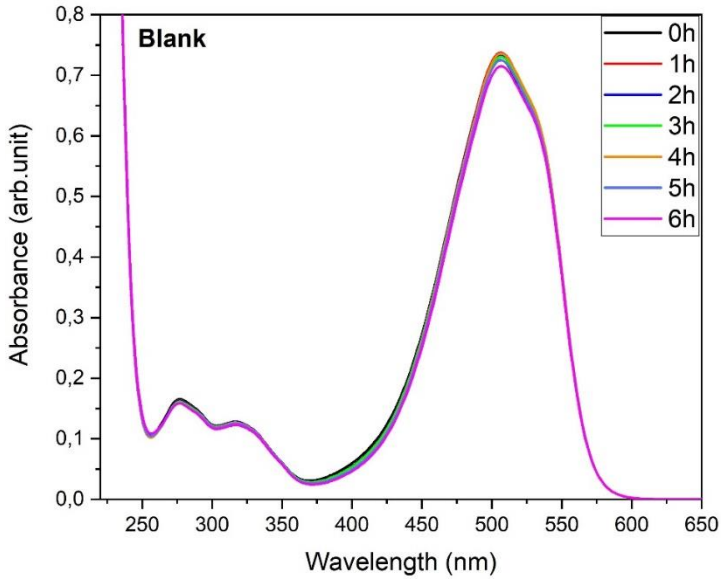

Figure IV. 6 UV–Vis absorption spectra of Methyl Orange solution without our thin films (blank)

IV.2.2. Photocatalytic degradation measurement

Figure IV.7 shows the absorption spectrum of the Methyl Orange solution exposed to UV-A light for 6 hours with our dipped samples in it that were prepared at different PH precursor values.

This figure clearly shows that the intensity of the absorption peaks decreases with the period of time that the solution is exposed to UV-A radiation, which indicates the MO has degraded. As can be seen, the absorption peak intensity changed as the PH precursor values varied, and a minimum value of peak intensity was found for all samples at 6 hours. It was noticed that the as-deposited TiO_2 thin films with a PH precursor value of 2.5, and 10.5, had the lowest value of Methyl Orange absorption intensity. However, the annealed TiO_2 thin film at PH=10.5, the absorption intensity reaches its maximum amount. As a result, it can be concluded that when thin films are used with a PH=2.5 and PH=10.5 (as-deposited samples), the decomposition of the Methyl Orange pigment is significant.

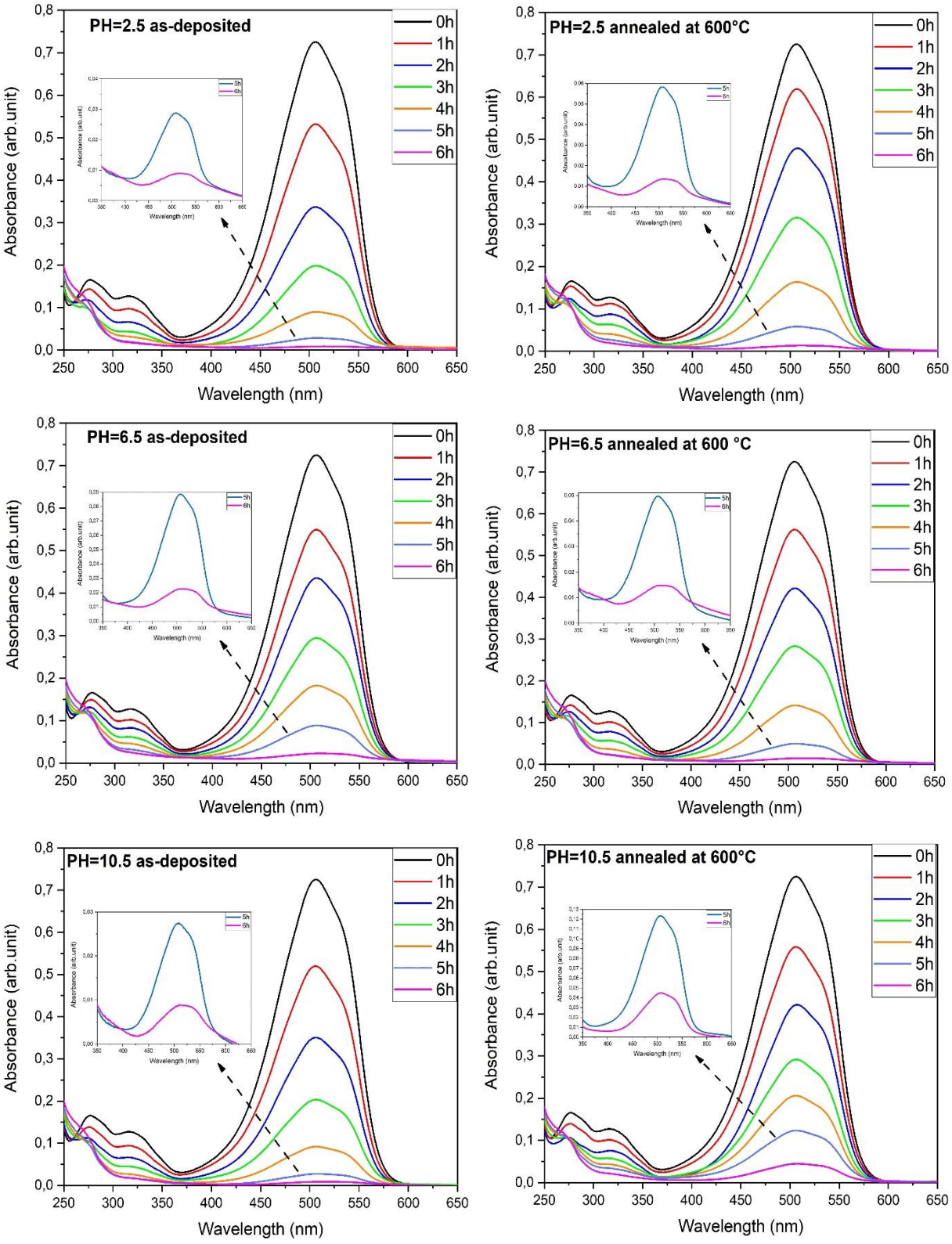

Figure IV. 7 UV–Vis absorption spectra of Methyl Orange solution with our dipped TiO_2 samples elaborated in different PH precursor as-deposited , and annealed at 600°C

IV.2.3. Photodegradation rate

For the photocatalytic degradation of organic pollutant dye solution, the photodegradation rate (PDR) of thin films was determined using the formula: [31,36]

$$PDR = \frac{C_t}{C_0} \times 100 \qquad \text{(IV.1)}$$

Where C_0 is the Concentration of Methyl Orange dye solution before the illumination, and C_t is the concentration of Methyl Orange dye after UV-A irradiation exposure time t.

Figure IV.8 shows the variation of photodegradation rate as a function of UV-A irradiation exposure time:

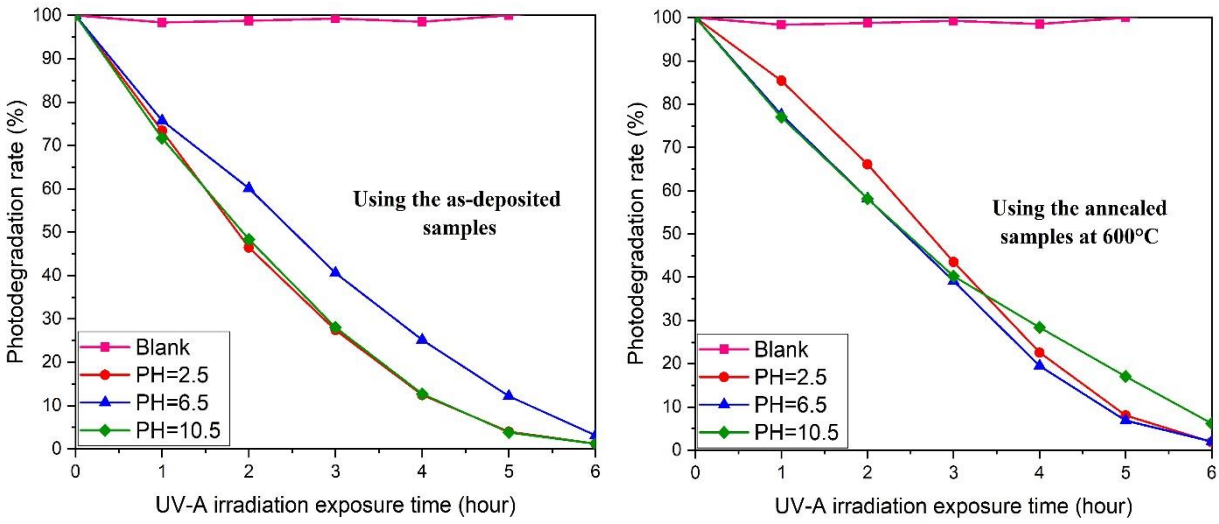

Figure IV. 8 Variation of photodegradation rate as a function of UV-A irradiation exposure time

The photodegradation rate at 6th hour values as a function of PH precursor solution values are shown in table IV.3: (it is worth noting that the Methyl Orange (MO) concentration at 0 hour is 100 %)

Table IV. 3 The photodegradation rate at 6th hour as a function of PH precursor values

PH precursor solution	Photodegradation rate at 6th hour (%)	
	As-deposited	Annealed at 600°C
PH=2.5	1.20	1.86
PH=6.5	3.12	2.01
PH=10.5	1.19	6.18

Table IV.3 shows the photodegradation rate of Methyl Orange. The lowest value of photodegradation rate was at PH=2.5, and PH=10.5, the as-deposited samples, this mean that the decrease in MO concentration was high. While we achieved the highest value at the PH precursor value PH=10.5, but at the annealed sample, this means that the decrease in MO concentration was low.

The following figure shows the color degradation of Methyl Orange using our samples:

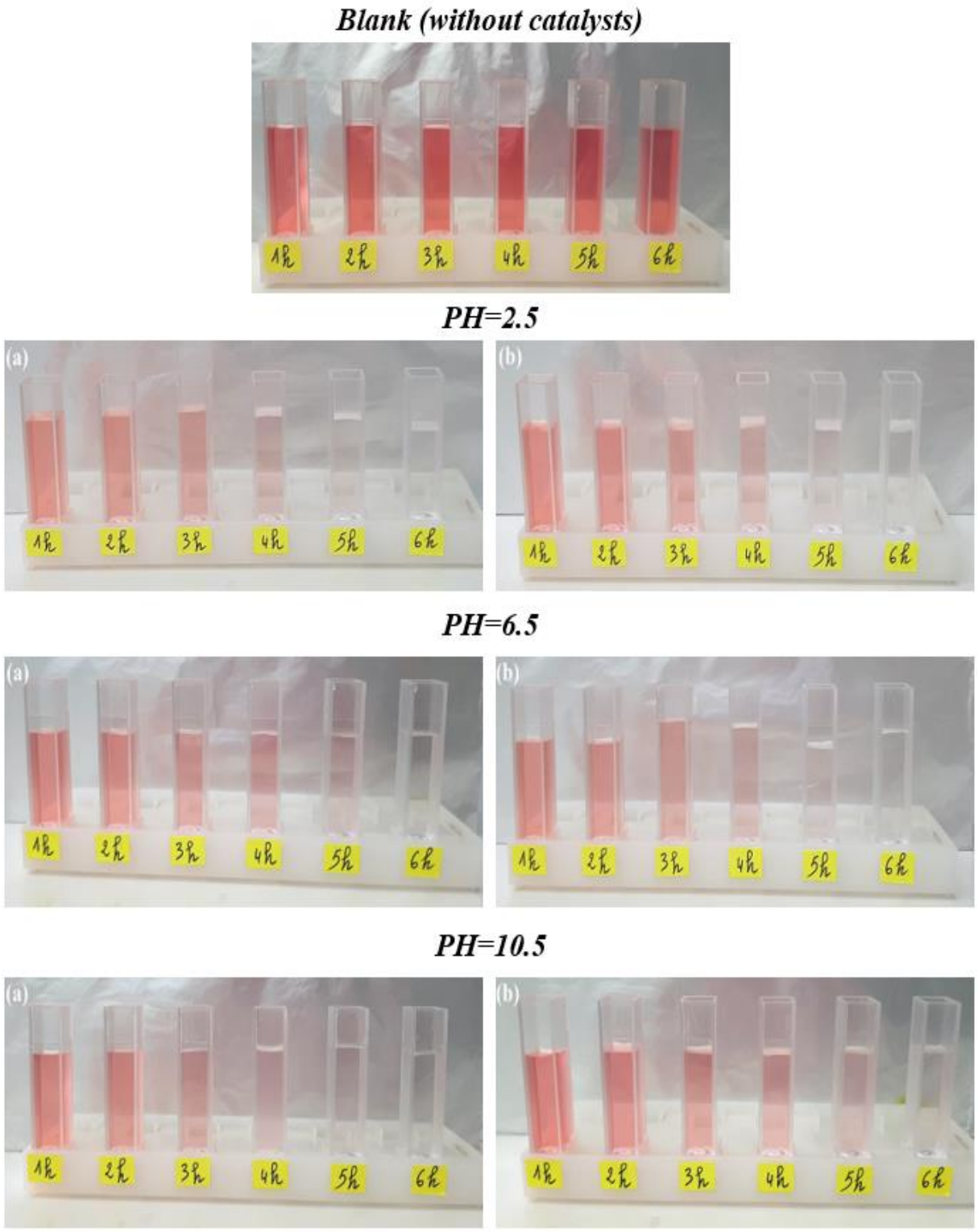

Figure IV. 9 Color degradation of Methyl Orange solution with catalysts (our TiO_2 thin films), and blank
(a) before annealing , (b) after annealing

IV.2.4.Photocatalytic reaction rate constant (k_{app})

Methyl Orange degradation under UV-A irradiation light is known to follow first order kinetics, i.e., the integrated band area (A) depends on time as follows: [38]

$$C_t = C_0 e^{-K_{app} t} \quad \text{(IV.1)}$$

Where: K_{app} is the constant of photocatalytic reaction rate.

The photocatalytic reaction rate constant (k_{app}) is the linear fit slope of the plot: ln (C_t/C_0) over time, and it was calculated from the following equation: [31]

$$-\ln\left[\frac{C_t}{C_0}\right] = K_{app} \times t \quad \text{(IV.2)}$$

The photocatalytic reaction rate constant (k_{app}) represented in Figure IV.10. We made the linear approximation of the curves and then calculated the slope from it.

It can be seen that the higher slope of the photocatalytic reaction rate plot, was at the as-deposited thin films, at PH precursor value equal to 2.5, and 10.5, it's the samples that have the best photodegradation of Methyl Orange (see table IV.3).

The K_{app} parameter represents the response time. The reaction speed on the surface of the thin films increases as the K_{app} values increase, which causes the Methyl Orange dye to degrade more quickly. [21]

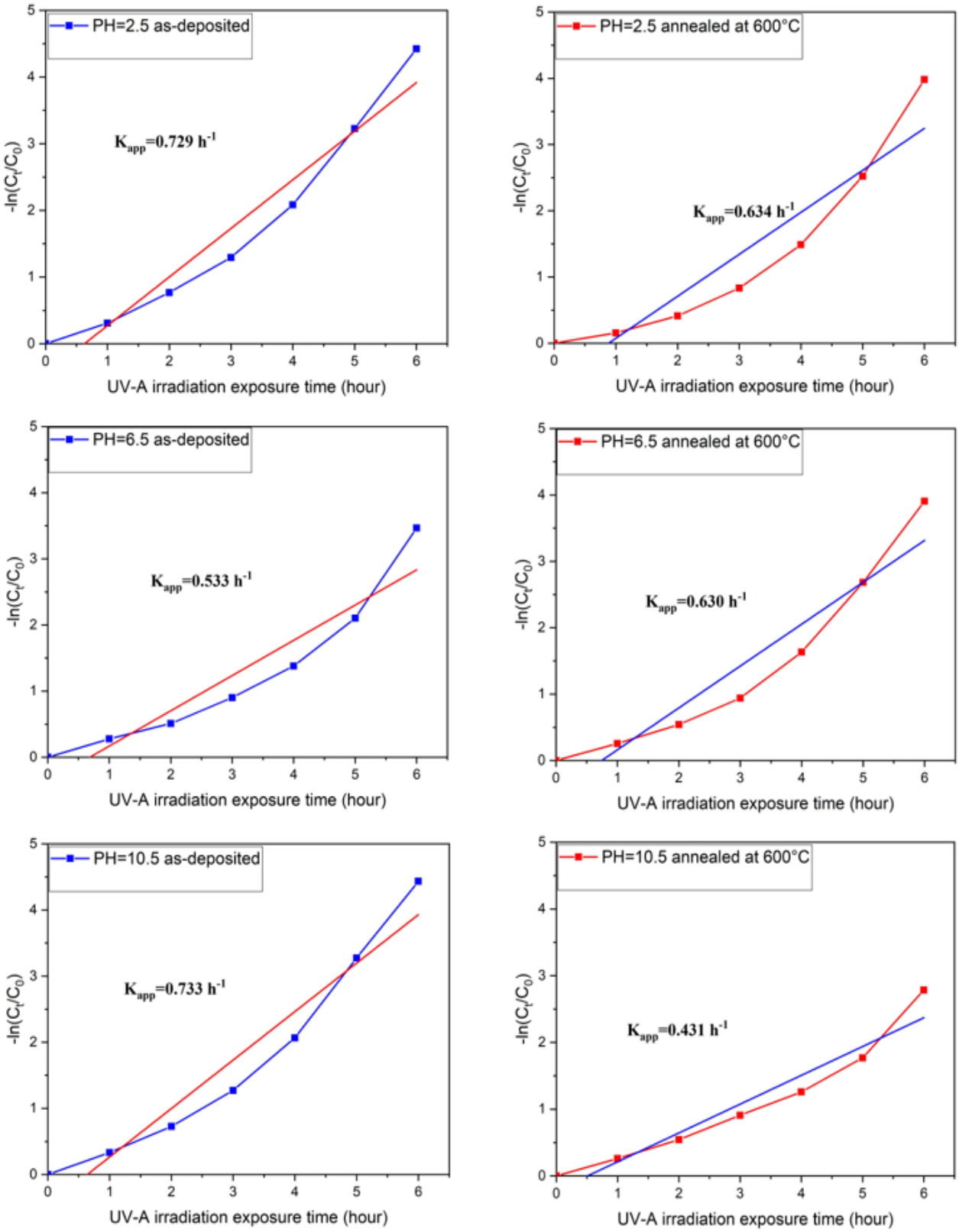

Figure IV. 10 Variation of $[-ln\ (C_t\ /C_0)]$ as a function of UV-A irradiation exposure time

General conclusion

The work discussed in this memory was primarily concerned the effect of PH precursor on the properties of our TiO_2 thin films deposited by ultrasonic spray process and their photocatalytic applications.

We have demonstrated the effect of PH on the structural, morphological, and optical properties of TiO_2 thin films using the following techniques: X-Rays diffraction, Raman spectroscopy, Field Emission Scanning Electron Microscopy FESEM, ATR-FTIR, UV-Vis-NIR, and Photoluminescence spectroscopy, and also for the photocatalytic application.

According to the results, we can obtain that:

- The PH affects the growth rate of our thin films.

- From XRD characterization we can obtain:

- The thin films of TiO_2 obtained before and after annealing at 600°C crystallize in the anatase phase with many orientations, confirm that the films are polycrystalline, with a preferential orientation along the (101) plane.
- The acidic medium has more crystallinity than the basic medium, and we can assume that after annealing the crystallinity is improved.
- At a low PH value (PH=2.5), has the biggest crystallite size, which means the dislocation density in this medium low.

- From the Raman spectra, we can confirm the results obtained from XRD, and that at PH=6.5 has the best crystallinity.

- From the FESEM characterization we can obtain that:

- All the samples of TiO_2 elaborated in different PH precursor values before and after annealing, have homogeneous, smoothing surfaces, and uniform grain sizes, without cracks, and pinholes.
- At PH=6.5, the thin film is denser than the other mediums, and that is confirmed by the XRD results too.

- ATR-FTIR spectra shows the appearance of the peaks that indicates the successful formation of TiO_2, and confirm the good adhesion between the glass substrate and the TiO_2 thin films.

The optical characterizations allow as to know:

- From UV-Vis-NIR characterization we can obtain that:

- The average of transmittance is about 85%.
- The band gap energy Eg varies depending the PH precursor solution, before and after annealing.
- The band gap energy Eg related to the crystalline state, the samples that have the best crystallinity, have the lowest value of Eg.
- The Urbach energy E_u is high when the degree of crystallinity is weak.

- From photoluminescence we can obtain that:

- The intensity of the peaks is related to the organization in the forbidden band gap, when the intensity is high, the number of defects in the forbidden band gap is fewer.
- The shift in the intense peak in the visible range is according to the bang gap energy values.

- We can say that after applying the photocatalytic application (water treatment) to our TiO_2 samples, the Methyl Orange was successfully degraded and its concentration was reduced from 100% to around 1%, after being exposed to 6 consecutive hours of simulated solar light irradiation (UV-A).

- We find that the photocatalytic performance is affected by the PH precursor solution, and it has the best result with samples deposited PH=2.5, and PH=10.5 before annealing, and it can also be affected by the thickness of the films.

After the success of using our elaborated thin films in the photocatalytic application, we can confirm that our TiO_2 thin films are suitable for industrial applications, and in the future, it is possible to improve their properties and apply them in several other applications such as: Hydrogen production, and gas sensors.

Annex

ASTM sheets for the TiO_2 anatase phase

Name and formula

Reference code:	00-021-1272
Mineral name:	Anatase, syn
Compound name:	Titanium Oxide
PDF index name:	Titanium Oxide
Empirical formula:	O_2Ti
Chemical formula:	TiO_2

Crystallographic parameters

Crystal system:	Tetragonal
Space group:	I41/amd
Space group number:	141
a (Å):	3,7852
:b (Å)	3,7852
:c (Å)	9,5139
:(°) Alpha	90,0000
:(°) Beta	90,0000
:(°) Gamma	90,0000
:Calculated density (g/cm^3)	3,89
:Volume of cell (10^6 pm^3)	136,31
:Z	4,00
:RIR	3,30

Subfiles and quality

Subfiles:	Alloy, metal or intermetalic Common Phase Corrosion Educational pattern Forensic Inorganic Mineral NBS pattern Pharmaceutical Pigment/Dye
Quality:	Star (S)

Comments

Color:	Colorless
Creation Date:	01/01/1970
Modification Date:	01/01/1970
Color:	Colorless
Additional Patterns:	See ICSD 9852 (PDF 01-071-1166)
Sample Source or Locality:	Sample obtained from National Lead Co., South Amboy, New Jersey, USA. Anatase and another polymorph, brookite (orthorhombic), are converted to rutile (tetragonal) by heating above 700 C. Pattern reviewed by Holzer, J., McCarthy, G., North Dakota State Univ, Fargo, North Dakota, USA, *ICDD Grant-in-Aid* (1990). Agrees well with experimental and calculated patterns
Additional Patterns:	Validated by calculated pattern
Temperature of Data Collection:	Pattern taken at 25 C.

References

Primary reference: *Natl. Bur. Stand. (U.S.) Monogr. 25*,) ,82 ,**7**1969(

Peak list

No.	h	k	l	d [A]	2Theta[deg]	I [%]
1	1	0	1	3,52000	25,281	100,0
2	1	0	3	2,43100	36,947	10,0
3	0	0	4	2,37800	37,801	20,0
4	1	1	2	2,33200	38,576	10,0
5	2	0	0	1,89200	48,050	35,0
6	1	0	5	1,69990	53,891	20,0
7	2	1	1	1,66650	55,062	20,0
8	2	1	3	1,49300	62,121	4,0
9	2	0	4	1,48080	62,690	14,0
10	1	1	6	1,36410	68,762	6,0
11	2	2	0	1,33780	70,311	6,0
12	1	0	7	1,27950	74,031	2,0
13	2	1	5	1,26490	75,032	10,0
14	3	0	1	1,25090	76,020	4,0
15	0	0	8	1,18940	80,727	2,0
16	3	0	3	1,17250	82,139	2,0
17	2	2	4	1,16640	82,662	6,0
18	3	1	2	1,16080	83,149	4,0
19	2	1	7	1,06000	93,221	2,0
20	3	0	5	1,05170	94,182	4,0
21	3	2	1	1,04360	95,143	4,0
22	1	0	9	1,01820	98,319	2,0
23	2	0	8	1,00700	99,804	2,0
24	3	2	3	0,99670	101,221	2,0
25	3	1	6	0,95550	107,448	4,0
26	4	0	0	0,94640	108,963	4,0
27	3	0	7	0,92460	112,841	2,0
28	3	2	5	0,91920	113,861	2,0
29	4	1	1	0,91380	114,909	2,0
30	2	1	9	0,89660	118,439	4,0
31	2	2	8	0,88900	120,104	2,0
32	4	1	3	0,88190	121,725	2,0
33	4	0	4	0,87930	122,336	2,0
34	4	2	0	0,84640	131,036	2,0
35	3	2	7	0,83080	135,998	2,0
36	4	1	5	0,82680	137,391	4,0

37	3	0	9	0,81020	143,888	2,0
38	4	2	4	0,79740	150,039	4,0
39	0	0	12	0,79280	152,634	2,0

Stick Pattern

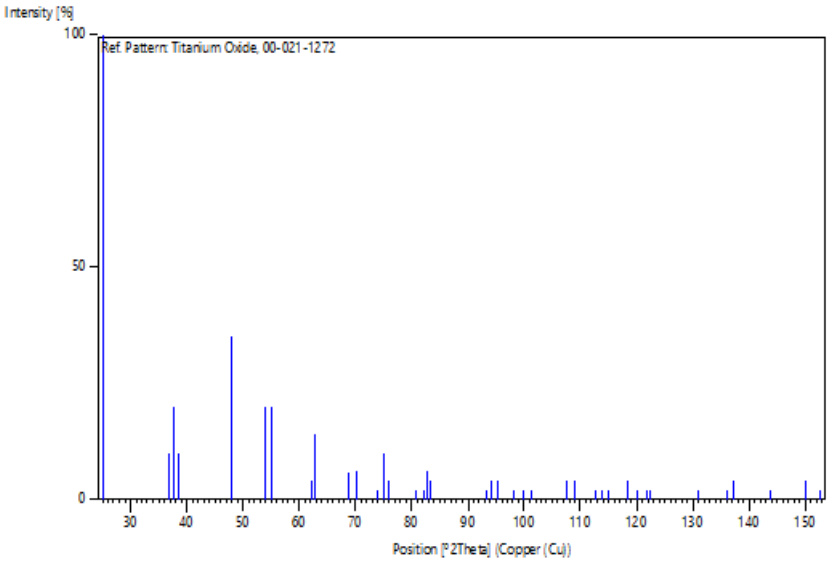

References

[1] Dahnoun, M., Attaf, A., Saidi, H., Benatia, R., Yahia, A., Khelifi, C., ... & Guerbous, L. (2018). *High transparent titanium dioxide-anatase thin films deposited by spin coating technique: Effect of annealing temperature*. Journal of Nanoelectronics and Optoelectronics, 13(9), 1359-1365.

[2] Zeribi, F., Attaf, A., Derbali, A., Saidi, H., Benmebrouk, L., Aida, M. S., ... & Ezzaouia, H. (2022). *Dependence of the physical properties of titanium dioxide (TiO_2) thin films grown by sol-gel (spin-coating) process on thickness*. ECS Journal of Solid State Science and Technology, 11(2), 023003.

[3] Khelifi, C. (2018). *Tin dioxide SnO_2 thin films deposited by ultrasonic spray technique: Properties and Applications* (Doctoral dissertation, University of Med Khider Biskra).

[4] Adjimi, A., & Attaf, N. (2022). *Elaboration des oxydes transparents conducteurs par voie Sol-Gel* (Doctoral dissertation, Université Frères Mentouri-Constantine 1).

[5] Hamrit, S., & Djessas, K. (2017). *Optimisation des dépôts sur des substrats flexibles d'oxydes transparents conducteurs nanostructurés à base de ZnO* (Doctoral dissertation).

[6] Idris, M. M., Olarinoye, I. O., Kolo, M. T., & Ibrahim, S. O. (2022). *Transparent conducting oxides thin film dosimetry: Present and the future.*

[7] Chala, S. (2017). L' effet de dopage par l'aluminium sur les propriétés des couches minces du TiO_2 élaborées par voie Sol-Gel (spin caoting). *Mémoire de Master, Université de Biskra*, 26.

[8] Pustovalova, A. A., Pichugin, V. F., Ivanova, N. M., & Bruns, M. (2017). *Structural features of N-containing titanium dioxide thin films deposited by magnetron sputtering*. Thin solid films, 627, 9-16.

[9] Goudjil, T. (2013). *Etude de l'oxyde de titane en couches minces en hétérojonction avec le silicium, application photovoltaîque* (Doctoral dissertation, Université Mouloud Mammeri)

[10] Messemeche, R., Saidi, H., Attaf, A., Benkhetta, Y., Chala, S., Azizi, R., & Nouadji, R.

(2020). *Elaboration and characterization of nano-crystalline layers of transparent titanium dioxide (Anatase-TiO_2) deposited by a sol-gel (spin coating) process*. Surfaces and Interfaces, 19, 100482.

[11] Dubrovinskaia, N. A., Dubrovinsky, L. S., Ahuja, R., Prokopenko, V. B., Dmitriev, V.,

Weber, H. P., ... & Johansson, B. (2001). *Experimental and theoretical identification of a new high-pressure TiO_2 polymorph*. Physical Review Letters, 87(27), 275501.

[12] Bokhimi, X., Morales, A., Aguilar, M., Toledo-Antonio, J. A., & Pedraza, F. (2001).

Local order in titania polymorphs. International journal of hydrogen energy, *26*(12), 1279-1287.

[13] Bouachiba, Y. (2014). *Contribution à l'élaboration de l'oxyde de titane par le procédé*

sol-gel: Effet du dopage et des conditions expérimentales. Université de Constantine, 1.

[14] Ertuğrul, G. (2016). *Investigation and characterization of ph effect on TiO_2 thin film*

surface (Master's thesis, Fen Bilimleri Enstitüsü).

[15] Eddah, M. (2020). *Dépôt et caractérisation de dispositifs photocatalytiques à base de*

TiO_2 pour traitement de l'eau (Doctoral dissertation, Maîtrise en sciences de l'énergie et des matériaux).

[16] Lin, C. P., Chen, H., Nakaruk, A., Koshy, P., & Sorrell, C. C. (2013). *Effect of annealing*

temperature on the photocatalytic activity of TiO2 thin films. Energy Procedia, 34, 627-636.

[17] Latrous, K., & Berkani, O. (2017). *Elaboration et caracterisation de couches minces*

d'oxyde de titane par la methode sol-gel.

[18] Nora, H. (2019). *Elaboration et caractérisation des couches minces d'oxyde de titane*

dopé Sn.

[19] Benkhetta, O. (2019). *Effet de la concentration de la solution sur les propriétés des*

couches minces de dioxyde de titane déposées par spray pyrolyse ultrasonique. Mémoire de master en physique, Université mohamed khider de biskra.

[20] Wang, Y. H., Rahman, K. H., Wu, C. C., & Chen, K. C. (2020). *A review on the pathways of the improved structural characteristics and photocatalytic performance of titanium dioxide (TiO_2) thin films fabricated by the magnetron-sputtering technique*. Catalysts, 10(6), 598.

[21] Messemeche, R. (2021). *Elaboration and characterization of undoped and doped titanium dioxide thin layers by sol gel (spin coating) for photocatalytic applications* (Doctoral dissertation, Université de mohamed kheider biskra).

[22] Haider, A. J., Jameel, Z. N., & Al-Hussaini, I. H. (2019). *Review on: titanium dioxide applications*. Energy Procedia, 157, 17-29.

[23] Adomnitei, C., Luca, D., Girtan, M., Sandu, I., Nica, V., Sandu, A. V., & Mardare, D. (2013). *Nb-doped TiO_2 thin films deposited by spray pyrolysis method*. Journal of Optoelectronics and Advanced Materials, 15(5-6), 519-522.

[24] Takeuchi, M., Sakamoto, K., Martra, G., Coluccia, S., & Anpo, M. (2005). *Mechanism of photoinduced superhydrophilicity on the TiO_2 photocatalyst surface*. The journal of physical chemistry B, 109(32), 15422-15428.

[25] Byrne, J. A., Eggins, B. R., Brown, N. M. D., McKinney, B., & Rouse, M. (1998). *Immobilisation of TiO_2 powder for the treatment of polluted water*. Applied Catalysis B: Environmental, 17(1-2), 25-36.

[26] Boujday, S., Wünsch, F., Portes, P., Bocquet, J. F., & Colbeau-Justin, C. (2004). *Photocatalytic and electronic properties of TiO_2 powders elaborated by sol–gel route and supercritical drying*. Solar Energy Materials and Solar Cells, 83(4), 421-433.

[27] Liu, S. M., Gan, L. M., Liu, L. H., Zhang, W. D., & Zeng, H. C. (2002). *Synthesis of single-crystalline TiO_2 nanotubes*. Chemistry of materials, 14(3), 1391-1397.

[28] Roy, P., Berger, S., & Schmuki, P. (2011). TiO_2 nanotubes: *synthesis and applications*. Angewandte Chemie International Edition, 50(13), 2904-2939.

[29] Zhao, Y., Li, C., Liu, X., Gu, F., Jiang, H., Shao, W., ... & He, Y. (2007). *Synthesis and optical properties of TiO_2 nanoparticles*. Materials Letters, 61(1), 79-83.

[30] Hanane, S., & Abdallah, A. (2022). *Effect of Doping with Niobium on the Properties of Titanium Dioxide Thin Films Prepared by Sol Gel (Spin-coating) Process*. AIJR Abstracts, 171-173.

[31] Messemeche, R., Benkhetta, Y., Attaf, A., Saidi, H., Aida, M. S., & Ben Khetta, O. (2022). *Photocatalytic mechanisms reactions of gallium doped TiO_2 thin films synthesized by sol gel (spin coating) in the degradation of methylene blue (MB) dye under sunlight irradiation*. Reaction Kinetics, Mechanisms and Catalysis, 135(5), 2735-2747.

[32] نور الهدى جحيش. *Effect of Niobium doping on the properties of Titanium Dioxide (TiO_2) Thin films elaborated by Sol-Gel (Spin-coating).*

[33] amel guettaf. *L'effet du dopage par l'étain sur les propriétés des couches minces de TiO_2 élaborées par voie sol-gel (sping-coating)*

[34] Benkheta, Y. (2019). *Elaboration and characterization of thin layers of zinc oxide (ZnO) deposited by ultrasonic spray for photovoltaic and optoelectronic applications* (Doctoral dissertation, University Mohamed Khider of Biskra).

[35] Mishra, D., Greving, D., Confalonieri, G. B., Perlich, J., Toperverg, B. P., Zabel, H., & Petracic, O. (2014). *Growth modes of nanoparticle superlattice thin films*. Nanotechnology, 25(20), 205602.

[36] Andronic, L., & Duta, A. (2007). *TiO_2 thin films for dyes photodegradation*. Thin solid films, 515(16), 6294-6297.

[37] Uppal, T., Reganti, S., Martin, E., & Verma, S. C. (2022). *Surface Inactivation of Human Coronavirus by MACOMA™ UVA-TiO2 Coupled Photocatalytic Disinfection System*. Catalysts, 12(7), 690.

[38] Dundar, I., Mere, A., Mikli, V., Krunks, M., & Oja Acik, I. (2020). *Thickness effect on photocatalytic activity of TiO_2 thin films fabricated by ultrasonic spray pyrolysis*. Catalysts, 10(9), 1058.

[39] Das, B. K. (2021). *Growth of ZnO Thin Film on Silicon and Glass Substrate by Pulsed Laser Deposition Technique*. Available at SSRN 3840984.

[40] Benamra, H., Saidi, H., Attaf, A., Aida, M. S., Derbali, A., & Attaf, N. (2020). *Physical properties of Al-doped ZnS thin films prepared by ultrasonic spray technique*. Surfaces and Interfaces, 21, 100645.

[41] Kherchachi, I. B., Attaf, A., Saidi, H., Bouhdjer, A., Bendjedidi, H., Benkhetta, Y., & Azizi, R. (2016). *Structural, optical and electrical properties of Sn_xS_y thin films grown by spray ultrasonic.* Journal of Semiconductors, 37(3), 032001.

[42] Suda, Y., Kawasaki, H., Ueda, T., & Ohshima, T. (2004). *Preparation of high quality nitrogen doped TiO_2 thin film as a photocatalyst using a pulsed laser deposition method*. Thin solid films, 453, 162-166.

[43] Heo, C. H., Lee, S. B., & Boo, J. H. (2005). *Deposition of TiO_2 thin films using RF magnetron sputtering method and study of their surface characteristics*. Thin solid films, 475(1-2), 183-188.

[44] Baghriche, L., & Aida, M. S. (2017). *Elaboration et caractérisation des couches minces d'oxyde de zinc et sulfure de zinc préparées par spray ultrasonique*.

[45] Jackson, T. J., & Palmer, S. B. (1994*). Oxide superconductor and magnetic metal thin film deposition by pulsed laser ablation: a review*. Journal of Physics D: Applied Physics, 27(8), 1581.

[46] Ashfold, M. N., Claeyssens, F., Fuge, G. M., & Henley, S. J. (2004). *Pulsed laser ablation and deposition of thin films*. Chemical Society Reviews, 33(1), 23-31.

[47] Jain, N. K., Sawant, M. S., Nikam, S. H., & Jhavar, S. (2016). *Metal deposition: Plasma-based processes.* Encyclopedia of Plasma Technology, 722-740.

[48] Znaidi, L. (2010). *Sol–gel-deposited ZnO thin films: A review*. Materials Science and Engineering: B, 174(1-3), 18-30.

[49] Bokov, D., Turki Jalil, A., Chupradit, S., Suksatan, W., Javed Ansari, M., Shewael, I. H., ... & Kianfar, E. (2021). *Nanomaterial by sol-gel method: synthesis and application*. Advances in Materials Science and Engineering, 2021, 1-21.

[50] Ardekani, S. R., Aghdam, A. S. R., Nazari, M., Bayat, A., Yazdani, E., & Saievar-Iranizad, E. (2019). *A comprehensive review on ultrasonic spray pyrolysis technique: Mechanism, main parameters and applications in condensed matter*. Journal of Analytical and Applied Pyrolysis, 141, 104631.

[51] Abderazzek, S., & Zitouni, K. (2022). *L'influence de dopage sur les propriétés des oxydes transparents* (Doctoral dissertation, university of M'sila).

[52] Attaf, A., Derbali, A., Saidi, H., Bouhdjer, A., Aida, M. S., Messemeche, R., ... & Djehiche, N. E. (2022). *Precursor concentration effect on the physical properties of transparent titania (Anatase-TiO_2) thin films grown by ultrasonic spray process for optoelectronics application*. Optical Materials, 132, 112790.

[53] Falcony, C., Aguilar-Frutis, M. A., & García-Hipólito, M. (2018). *Spray pyrolysis technique; high-K dielectric films and luminescent materials: a review*. Micromachines, 9(8), 414.

[54] Bunaciu, A. A., UdriŞTioiu, E. G., & Aboul-Enein, H. Y. (2015). *X-ray diffraction: instrumentation and applications*. Critical reviews in analytical chemistry, 45(4), 289-299.

[55] Epp, J. (2016). *X-ray diffraction (XRD) techniques for materials characterization*. In Materials characterization using nondestructive evaluation (NDE) methods (pp. 81-124). Woodhead Publishing.

[56] Khelifi, C., Attaf, A., Yahia, A., & Dahnoun, M. (2019). *Investigation of F doped SnO_2 thin films properties deposited via ultrasonic spray technique for several applications*. Surfaces and Interfaces, 15, 244-249.

[57] Attaf, A., Djadai, A., Derbali, A., Saidi, H., Aida, M. S., Lehraki, N., ... & Poulain, M. (2022). *The effect of ultrasonic wave amplitude on the physical properties of zinc oxide (ZnO) deposited by ultrasonic spray method*. Materials Science and Engineering: B, 275, 115525.

[58] Juma, A. O., Acik, I. O., Mikli, V., Mere, A., & Krunks, M. (2015). *Effect of solution composition on anatase to rutile transformation of sprayed TiO_2 thin films*. Thin Solid Films, 594, 287-292.

[59] Yahia, A. (2020). *Optimization of indium oxide thin films properties prepared by sol gel spin coating process for optoelectronic applications* (Doctoral dissertation, University Mohamed Khider of Biskra).

[60] Messemeche, R. (2016). *Caractérisation de couches minces d'oxyde de titane (TiO_2) Obtenues par Sol Gel (Spin coating): L'effet de la concentration de la solution*. Mémoire de master, Université Med Khider-Biskra, 10.

[61] Uddin, M. G. (2018). *Development of Simplified In Situ Processing Routes for Rear-Side Patterning of Silicon Heterojunction Interdigitated Back Contact (SHJ-IBC) Solar Cells* (Master's thesis, Itä-Suomen yliopisto).

[62] Karbiche Aicha, T. R. *L'effet des solvants sur les propriétés des couches minces du TiO_2 élaborées par spray pyrolyse ultrasonique.*

[63] Arunachalam, A., Dhanapandian, S., Manoharan, C., & Sivakumar, G. (2015). *Physical properties of Zn doped TiO2 thin films with spray pyrolysis technique and its effects in antibacterial activity*. Spectrochimica Acta Part A: Molecular and Biomolecular Spectroscopy, 138, 105-112.

[64] Nasr, T. B., Kamoun, N., Kanzari, M., & Bennaceur, R. (2006). *Effect of PH on the properties of ZnS thin films grown by chemical bath deposition. Thin solid films*, 500(1-2), 4-8.

[65] Bouhdjer, A., Attaf, A., Saidi, H., Bendjedidi, H., Benkhetta, Y., & Bouhaf, I. (2015). *Correlation between the structural, morphological, optical, and electrical properties of In_2O_3 thin films obtained by an ultrasonic spray CVD process*. Journal of Semiconductors, 36(8), 082002.

[66] Krishnan, V. G., Elango, P., Ganesan, V., & Sathish, P. (2016). *PH deeds on structural, optical, electrical and gas sensing performance of TiO_2 nanofilms by automated nebulizer spray pyrolysis technique*. Optik, 127(23), 11102-11110.

[67] Chibani, O., Touam, T., Chelouche, A., & Ouarez, L. (2018). *Investigation of the effects of acidic PH and annealing on the properties of nanostructured TiO_2 thin films for waveguiding applications.* Journal of Alloys and Compounds, 768, 866-874.

[68] Aida, I. S., & Sreekantan, S. (2011). *Effect of PH on TiO_2 nanoparticles via sol-gel method.* In Advanced Materials Research (Vol. 173, pp. 184-189). Trans Tech Publications Ltd.

[69] Chen, X., & Mao, S. S. (2007). *Titanium dioxide nanomaterials: synthesis, properties, modifications, and applications*. Chemical reviews, 107(7), 2891-2959.

[70] Nouadji, R. (2022). *Elaboration and characterization of undoped and doped indium oxide thin layers elaborated by sol gel process for photonic and photovoltaic applications* (Doctoral dissertation, Université de mohamed kheider biskra).

[71] Miranda, S., Vilanova, A., Lopes, T., & Mendes, A. (2017). *TiO_2-coated window for facilitated gas evolution in PEC solar water splitting*. RSC advances, 7(47), 29665-29671.

[72] Noori, L., Hoseinpour, V., & Shariatinia, Z. (2022). *Optimization of TiO_2 paste concentration employed as electron transport layers in fully ambient air processed perovskite solar cells with a low-cost architecture*. Ceramics International, 48(1), 320-336.

[73] Houng, B., Huang, C. L., & Tsai, S. Y. (2007). *Effect of the PH on the growth and properties of sol–gel derived boron-doped ZnO transparent conducting thin film*. Journal of Crystal Growth, 307(2), 328-333.

[74] Mathews, N. R., Morales, E. R., Cortés-Jacome, M. A., & Antonio, J. T. (2009). *TiO_2 thin films–Influence of annealing temperature on structural, optical and photocatalytic properties*. Solar energy, 83(9), 1499-1508.

Abstract

Effect of PH precursor on the properties of TiO_2 thin films deposited by ultrasonic spray process and their photocatalytic applications

In this memory, we study the effect of PH precursor on the structural, morphological, and optical properties of titanium dioxide TiO_2 thin films before and after annealing, deposited by the ultrasonic spray process, and their photocatalytic applications. To characterize these samples, we use for the structural characterizations: X-Rays Diffractions (XRD), Raman and ATR-FTIR spectroscopy, for the morphological study we use FESEM, and for the optical characterizations, we use the UV-Vis-NIR and photoluminescence spectroscopy.

The XRD spectra show that all the samples have a polycrystalline structure with a favorable orientation growth plane (101) which refers to the anatase phase. The crystallite size is severely varied with the PH precursor. Our results confirm that the PH can affect the structure, and Raman spectra enhance these results.

The FESEM shows that all the thin films have a homogenous surface, and uniform grain size, without any cracks or pinholes.

The ATR-FTIR spectra confirm the successful formation of TiO_2 thin film and their good adhesion to the glass substrate.

The UV-Vis-NIR shows that our samples have a high transmittance in the visible range of around 85%, and the band gap energy Eg is affected by the PH precursor solution.

The photoluminescence allows us to know that the intensity of the peak is related to forbidden band gap purity from defects, when the number of defects between the conduction band and the valence band is fewer, the peaks have a high intensity. The intensity of these peaks is affected by the PH precursor of the solution and annealing temperature.

Our TiO_2 thin films have the ability to degrade Methyl Orange contaminant, and their photocatalytic activity under simulated solar light irradiation (UV-A) is very high, where the Methyl Orange concentration decreased from 100% to around 1%. The performance of TiO_2 thin film can enhance with PH precursor values equal to 2.5 and 10.5 (acidic and basic mediums).

Keywords: Titanium dioxide TiO_2, thin films, PH precursor, structural, morphological, and optical properties, ultrasonic spray process, photocatalytic application, Methyl Orange, simulated solar light irradiation (UV-A).

Résumé

Effet du précurseur de PH sur les propriétés des couches minces de TiO_2 déposées par la technique de spray ultrasonique et leurs applications photocatalytiques

Dans ce mémoire, nous étudions l'effet du précurseur de PH sur les propriétés structurales, morphologiques et optiques de couches minces de dioxyde de titane TiO_2 avant et après recuit, déposées par le procédé de spray ultrasonique, et leurs applications photocatalytiques. Pour caractériser ces échantillons, nous utilisons pour les caractérisations structurales : les diffractions des rayons X (DRX), la spectroscopie Raman et ATR-FTIR, pour l'étude morphologique nous utilisons le FESEM, et pour les caractérisations optiques, nous utilisons la spectroscopie UV-Vis-NIR et de photoluminescence.

Les spectres DRX montrent que tous les échantillons ont une structure polycristalline avec un plan de croissance d'orientation favorable (101) qui fait référence à la phase anatase. La taille des cristallites varie fortement avec le précurseur de PH. Nos résultats confirment que le PH peut affecter la structure, et les spectres Raman renforcent ces résultats.

Le FESEM montre que tous les films minces ont une surface homogène et une granulométrie uniforme, sans fissures ni piqûres.

Les spectres ATR-FTIR confirment la formation réussie de couches minces de TiO_2 et leur bonne adhésion au substrat de verre.

L'UV-Vis-NIR montre que nos échantillons ont une transmission élevée dans le domaine visible d'environ 85 %, et l'énergie de la bande interdite Eg est affectée par le PH précurseur de la solution.

La photoluminescence nous permet de savoir que l'intensité du pic est liée à la pureté de la bande interdite des défauts, lorsque le nombre de défauts entre la bande de conduction et la bande de valence est moindre, les pics ont une intensité élevée. L'intensité de ces pics est affectée par le précurseur PH de la solution et la température de recuit.

Nos couches minces de TiO_2 ont la capacité de dégrader le contaminant de méthylorange et leur activité photocatalytique sous irradiation solaire simulée (UV-A) est très élevée, où la concentration de Méthyl Orange est passée de 100 % à environ 1 %. Les performances du film mince de TiO_2 peuvent s'améliorer avec des valeurs de précurseur de PH égales à 2,5 et 10,5 (milieux acides et basiques)

Mots-clés : Dioxyde de titane TiO_2, couches minces, précurseur de PH, propriétés structurelles, morphologiques et optiques, technique de spray ultrasonique, application photocatalytique, Méthyl Orange irradiation solaire simulée (UV-A).

ملخص

تأثير درجة حموضة المحلول " الأس الهيدروجيني" على خصائص الشرائح الرقيقة لثنائي أكسيد التيتانيوم الموضعة بتقنية الرش بالموجات فوق الصوتيةً و تطبيقاتها في التحفيز الضوئي

في هذه المذكرة ، درسنا تأثير درجة حموضة المحلول " الأس الهيدروجيني" على الخصائص البنيوية والمورفولوجية والبصرية للأغشية الرقيقة لثنائي أكسيد التيتانيوم TiO_2 قبل وبعد المعالجة الحرارية ، الموضعة بتقنية الرش بالموجات فوق الصوتية ، وتطبيقاتها في التحفيزي الضوئي. لتوصيف هذه العينات ، استخدمنا للتوصيفات الهيكلية: انعراج الأشعة السينية (XRD) ، مطيافية Raman و ATR-FTIR ، للدراسة المورفولوجية استخدمنا المجهر الإلكتروني الماسح للانبعاثات الحقلية FESEM ، وللتوصيفات البصرية ، استخدمنا مطيافية UV-Vis-NIR ، و مطيافية اللمعان الضوئي photoluminescence.

يوضح أطياف انعراج الأشعة السينية X أن جميع العينات لها بنية متعدد البلورات مع اتجاه نمو مفضل يوافق (101) والذي يشير إلى تشكل طور الأناتاز anatase. يتغير حجم البلورات بشدة مع قيمة درجة حموضة المحلول " الأس الهيدروجيني". تؤكد نتائجنا أن الرقم الهيدروجيني يمكن أن يؤثر على البنية ، وتعزز أطياف رامان هذه النتائج.

يوضح المجهر الإلكتروني الماسح للانبعاثات الحقلية FESEM أن جميع الأغشية الرقيقة لها سطح متجانس ، وحجم حبيبات موحد ، بدون أي شقوق أو ثقوب.

تؤكد أطياف ATR-FTIR التكوين الناجح للفيلم الرقيق TiO_2 والتصاقها الجيد بالركيزة الزجاجية.

توضح مطيافية UV-Vis-NIR أن عيناتنا لها نفاذية عالية في النطاق المرئي بحوالي 85٪ ، وأن طاقة فجوة النطاق الممنوع Eg تتأثر بدرجة حموضة المحلول.

يتيح لنا اللمعان الضوئي photoluminescence معرفة أن شدة الذروة مرتبطة بنقاء فجوة النطاق الممنوع من العيوب ، عندما يكون عدد العيوب بين نطاق التوصيل ونطاق التكافؤ أقل ، يكون للذروة قيمة عالية . تتأثر شدة هذه الذروات بدرجة حموضة المحلول " الأس الهيدروجيني" ودرجة حرارة المعالجة الحرارية.

تتمتع أغشية TiO_2 الرقيقة الخاصة بنا بالقدرة على تحلل الملوثات الميثيل البرتقالية ، كما أن نشاطها التحفيزي الضوئي تحت إشعاع ضوء الشمس المحاكي (UV-A) مرتفع للغاية ، حيث انخفض تركيز الميثيل البرتقالي من 100٪ إلى حوالي 1٪. يمكن تحسين أداء فيلم TiO_2 الرقيق بقيم سلائف PH تساوي 2.5 و 10.5 (وسط حمضي وقاعدة).

تتمتع أغشية TiO_2 الرقيقة التي تم تحضيرها بالقدرة على تحليل و تفكيك ملوثات الميثيل البرتقالية ، كما أن نشاطها التحفيزي الضوئي تحت إشعاع ضوء الشمس المحاكي (UV-A) مرتفع للغاية ، حيث انخفض تركيز الميثيل البرتقالي من 100٪ إلى حوالي 1٪. يمكن تحسين أداء أغشية TiO_2 الرقيقة بقيم درجة حموضة تساوي 2.5 و 10.5 (وسط حمضي وقاعدي).

الكلمات المفتاحية: ثنائي أكسيد التيتانيوم TiO_2 ، الأغشية الرقيقة ، درجة الحموضة " الأس الهيدروجيني" ، الخصائص البنيوية ، المورفولوجية ، والبصرية ، تقنية الرش بالموجات فوق الصوتية ، تطبيق التحفيز الضوئي ، ميثيل برتقالي ، تشعيع الضوء الشمسي المحاكى (UV-A).